ISSN 0869-5911, Petrology, 2006, Vol. 14, No. 4, pp. 361–389. © Pleiades Publishing, Inc., 2006.
Original Russian Text © A.A. Arzamastsev, F. Bea, L.V. Arzamastseva, P. Montero, 2006, published in Petrologiya, 2006, Vol. 14, No. 4, pp. 384–414.

Proterozoic Gremyakha–Vyrmes Polyphase Massif, Kola Peninsula: An Example of Mixing Basic and Alkaline Mantle Melts

A. A. Arzamastsev[a], F. Bea[b], L. V. Arzamastseva[a], and P. Montero[b]

[a]*Geological Institute, Kola Science Center, Russian Academy of Sciences, ul. Fersmana 14, Apatity, Murmansk oblast, 184209 Russia*
e-mail: arzamas@geokse.apatity.ru

[b]*University of Granada, Department of Mineralogy and Petrology, Fuentenueva s/n, 18002, Granada, Spain*

Received April 29, 2005

Abstract—The paper presents newly obtained data on the geological structure, age, and composition of the Gremyakha–Vyrmes Massif, which consists of rocks of the ultrabasic, granitoid, and foidolite series. According to the results of the Rb–Sr and Sm–Nd geochronologic research and the U–Pb dating of single zircon grains, the three rock series composing the massif were emplaced within a fairly narrow age interval of 1885 ± 20 Ma, a fact testifying to the spatiotemporal closeness of the normal ultrabasic and alkaline melts. The interaction of these magmas within the crust resulted in the complicated series of derivatives of the Gremyakha–Vyrmes Massif, whose rocks show evidence of the mixing of compositionally diverse mantle melts. Model simulations based on precise geochemical data indicate that the probable parental magmas of the ultrabasic series of this massif were ferropicritic melts, which were formed by endogenic activity in the Pechenga–Varzuga rift zone. According to the simulation data, the granitoids of the massif were produced by the fractional crystallization of melts genetically related to the gabbro–peridotites and by the accompanying assimilation of Archean crustal material with the addition of small portions of alkaline-ultrabasic melts. The isotopic geochemical characteristics of the foidolites notably differ from those of the other rocks of the massif: together with carbonatites, these rocks define a trend implying the predominance of a more depleted mantle source in their genesis. The similarities between the Sm–Nd isotopic characteristics of foidolites from the Gremyakha–Vyrmes Massif and the rocks of the Tiksheozero Massif suggest that the parental alkaline–ultrabasic melts of these rocks were derived from an autonomous mantle source and were only very weakly affected by the crust. The occurrence of ultrabasic foidolites and carbonatites in the Gremyakha–Vyrmes Massif indicates that domains of metasomatized mantle material were produced in the sublithospheric mantle beneath the northeastern part of the Fennoscandian Shield already at 1.88 Ga, and these domains were enriched in incompatible elements and able to produce alkaline and carbonatite melts. The involvement of these domains in plume–lithospheric processes at 0.4–0.36 Ga gave rise to the peralkaline melts that formed the Paleozoic Kola alkaline province.

DOI: 10.1134/S0869591106040035

INTRODUCTION

Most alkaline massifs typically consist of several phases of different composition, which were derived from one or more sources and then emplaced one after another. One of the main factors that controlled the origin of polyphase intrusive bodies was crystallization differentiation, which resulted in successive comagmatic series within a single massif. An example of massifs of this type is offered by carbonatite intrusions, which were produced by the successive emplacement of ultrabasic, alkaline, and carbonatite melts that belonged, judging from their petrographic and geochemical characteristics, to a single magmatic series. The polyphase character of the massifs could also result from the interaction of mantle and/or crustal sources of distinct composition and genesis that generated distinct magmatic series within a single massif. These intrusive bodies were emplaced in pericratonic environments, where conditions were favorable for the emplacement of magmas from various mantle levels.

Proterozoic rifting in the cratonization regions of the Archean basement of northeastern Fennoscandia produced the Pechenga–Varzuga volcanic–sedimentary belt (Mitrofanov et al., 1995, 1998), which was characterized by intense magmatic activity that started at 2.45 Ga and continued for more than 550 m.y. (Berthelsen and Marker, 1986; Sharkov and Smolkin, 1998). The closing phase of endogenic activity at ~1.9 Ga was associated with alkaline magmatism in the foreland of the rift structure. This time was marked by the origin of the large Gremyakha–Vyrmes alkaline massif 90 km southeast of the Pechenga structure (Fig. 1). Available

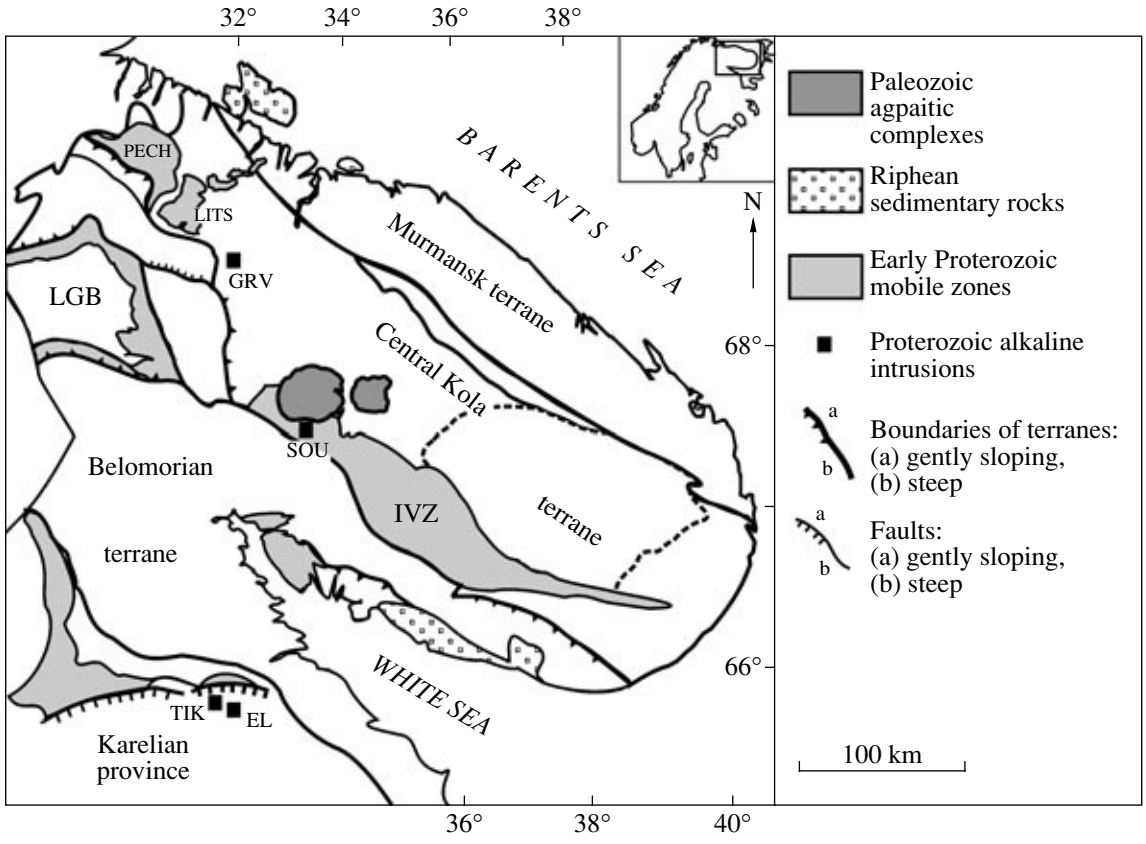

Fig. 1. Schematic map of Archean and Proterozoic terranes in the northeastern Baltic shield (modified after Balaganskii et al., 1998). Proterozoic alkaline intrusions: GRV—Gremyakha–Vyrmes, SOU—Soustova, EL—Elet'ozero, TIK—Tiksheozero. PECH—Pechenga zone, IVZ—Imandra–Varzuga zone, LGB—Lapland Granulite Belt, LITS—Litsa–Ara Guba granitoid complex.

isotopic dates (1.97–1.87 Ga; Savatenkov et al., 1998; Bea et al., 2001) indicate that this massif was emplaced immediately after magmatic events in the Pechenga structure.

The Gremyakha–Vyrmes Massif consists of a fairly contrasting group of rocks, which were formed by magmatic crystallization, the mixing of the parental melts, and contact interactions between discrete melt portions. There are known examples of massifs with combined foidolites, nepheline syenites, and alkaline granites, as well as widespread associations of ultrabasic rocks, foidolites, and carbonatites (Eby, 1985; Krivdik and Tkachuk, 1990; Kogarko et al., 1995). The Gremyakha–Vyrmes Massif includes the derivatives of three intrusive series (ultrabasic, granitoid, and foidolite), which makes this massif different from other polyphase alkaline intrusions.

Our research was centered on determining the conditions under which the compositionally distinct magmatic series of the Gremyakha–Vyrmes Massif were produced and on the genesis of these series. Our mineralogical–geochemical study included the determining of the isotopic characteristics of the major rock types of this massif. We identified "pure" magmatic rocks that did not undergo mixing and were not affected by contact metasomatic processes. Our results led us to propose a model for the genesis of the massif, including the interaction of magmatic melts derived from distinct mantle sources with one another and with crustal rocks. Below we also discuss the role of alkaline magmatism as a precursor of the development of the largest Paleozoic Kola alkaline province in northeastern Fennoscandia.

GEOLOGIC SETTING AND INNER STRUCTURE OF THE MASSIF

The Gremyakha–Vyrmes Massif in the Central Kola terrane (Balaganskii et al., 1998) in the central Kola Peninsula is hosted by mica and oligoclase granite-gneisses of the basement, which belong to the undifferentiated Late Archean Kola–Belomorian Complex (Mitrofanov et al., 1995). The central part of the Pechenga–Varzuga rift zone, situated west of the massif, was affected by intense meridional displacement during the Svecofennian orogeny (Berthelsen and Marker, 1986; Mitrofanov et al., 1995) (Fig. 1). The Gremyakha–Vyrmes Massif ~19 km long is spatially restricted to a large meridional weakened zone related to faults, along which the Early Proterozoic Pechenga and Imandra–Varzuga structures were displaced. The southern

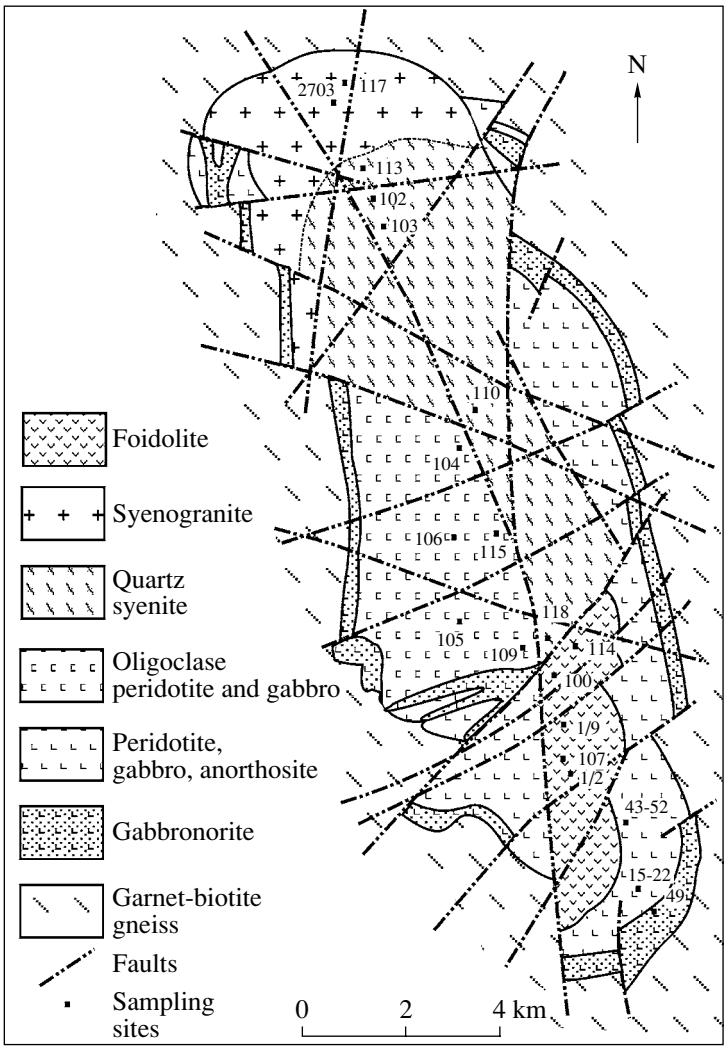

Fig. 2. Map of the Gremyakha–Vyrmes Massif (modified after Osokin, 1987 and with the use of data from Polkanov et al., 1967; Kukharenko et al., 1971; Vinogradov et al., 1985; Radchenko and Rezhenova, 1990).

flank of this belt hosts the Soustova intrusion, which was formed at 1872 ± 8 Ma by the interaction of fluidized alkaline melts with Archean basement rocks (Bea et al., 2001).

Geological data (Polkanov et al., 1967; Kukharenko et al., 1971; Vinogradov et al., 1985) indicate that the modern erosion level of the massif exposes three rock groups, and each of them is an independent intrusive body (Fig. 2). The rocks of the massif were emplaced in the following succession: (i) ultrabasic layered series, (ii) alkali granite series, and (iii) foidolite series. Ultrabasic rocks and granitoids compose two autonomous bodies, which are dominated in the massif, and alkaline rocks occur in its core along a submeridional fault (Fig. 2). The inner structure of the massif is significantly complicated by younger tectonics, which displaced large rock blocks of the aforementioned complexes.

ANALYTICAL TECHNIQUES

The 40 samples selected as representing all major rock varieties of the massif were analyzed for all major and 40 trace elements, including all REE; and 15 samples were additionally analyzed for Sr and Nd isotopic composition. The concentrations of major elements were determined by XRF. The analyses were carried out using rock powders fused with lithium tetraborate, accurate to no worse than ±1.5% at concentrations of 10%. Zr was determined by XRF accurate to at least ±4% for concentrations of 100 ppm. Trace elements were analyzed by ICP-MS on a PE SCIEX ELAN-5000 mass spectrometer with Rh as the internal standard. The preparation procedures of the samples involved the dissolution of 100 mg of the powders in an HNO_3 + HF mixture in a Teflon capsule at ~180°C for 30 min. After evaporation, the residues were dissolved in 100 ml of

Table 1. Modal composition of rock samples from the Gremyakha–Vyrmes Massif

Sample	Rock	Symbol	Modal composition (%)	Grain size	Structure
GV-19, GV-46, GV-49, GV-50, GV-52	Peridotite	PRD	Olivine (45–65), augite (25–35), titanomagnetite + ilmenite (10–25), apatite (5–10), spinel, kaersutite	Medium-grained to coarse-grained	Massive, with ore interlayers
GV-20	Plagioclase-bearing peridotite	PRDpl	Olivine (45), augite (25), plagioclase (8), titanomagnetite + ilmenite (20), apatite (2), spinel, kaersutite, garnet	Medium-grained	Massive
111/275	Plagioclase-bearing pyroxenite	PRXpl	Augite (19), hypersthene (24), titanomagnetite + ilmenite (12), plagioclase (4), olivine (0.2), apatite (6.6), kaersutite (27), biotite (6.5), garnet (0.5)	Medium-grained	Massive
GV-15, GV-43, GV-45, GV-51, GV-64, 113/279, 101/258	Gabbro	GBR	Plagioclase (32–46), hedenbergite (45–52), titanomagnetite + ilmenite (3–11), olivine (0–10), apatite (1–6), kaersutite, biotite	Coarse-grained	Massive
GV-22, 51/23	Olivine gabbro	GBRol	Olivine (15–25), augite (30), plagioclase (10–25), titanomagnetite + ilmenite (15), spinel, apatite (7), kaersutite (5), garnet	Coarse-grained	Massive
GV-44	Ore gabbro	GBRmt	Plagioclase (38), augite (20), titanomagnetite + ilmenite (32), olivine (3), spinel, apatite (4), kaersutite, biotite	Coarse-grained	Trachytoid
20/4	Leucogabbro	GBRA	Plagioclase (60), augite (10), titanomagnetite, ilmenite, olivine (1), apatite (4), kaersutite, biotite	Medium-grained	Massive
GV-105, GV-106, GV-115	Monzosyenite	GBRS	Oligoclase-perthite (or plagioclase and orthoclase) (65–75), hedenbergite (20–35), olivine (0–5), magnetite + ilmenite, apatite, quartz (0–3)	Coarse-grained	Massive
GV-104, GV-109, 5/1	Nepheline-bearing syenite (pulaskite)	GBRP	K–Na perthite (70–83), aegirine-augite (5–13), nepheline (1–4), biotite (4–7), olivine, amphibole, apatite	Medium-grained	Massive
GV-111	Nepheline-bearing gabbro (laurdalite)	LRD	Plagioclase (60), aegirine-augite (23), nepheline (5), biotite (6), kaersutite (4), apatite (1), magnetite, titanite	Medium-grained	Massive
GV-1/9A, GV-100	Foidolite	FOID	Aegirine-augite (30–45), nepheline (40–50), sodalite (0–5), biotite (7–9), orthoclase (1–2), kaersutite (1–2), apatite (0.5), magnetite (1–2), titanite (1)	Coarse-grained, pegmatoid	Massive
GV-1/2, GV-107	Foyaite	FOY	K–Na perthite (55–65), nepheline (20–25), aegirine-augite (5–10), biotite (3), apatite, magnetite, titanite, pyrochlore, zircon	Coarse-grained	Trachytoid
2703, GV-117, GV-113	Syenogranite	GRAN	Quartz (30), microcline (30), albite (30), aegirine (6), alkali amphibole (2), biotite (1), aenigmatite (1), titanite, apatite, zircon	Coarse-grained	Gneissose
GV-102, GV-103, GV-110, GV-118	Quartz syenite	GRAS	Quartz (17–18), microcline (27), albite (40), aegirine (3), alkali amphibole (10), aenigmatite (2), biotite, titanite, apatite, zircon	Coarse-grained	Gneissose

4% HNO_3. The analyses were conducted accurate to at least ±2 and ±5% for concentrations of 50 and 5 ppm, respectively.

Samples for the Sr and Nd isotopic research were decomposed following the aforementioned methods with the use of analytical-grade reactants and, upon chromatographic separation on ion exchangers, were analyzed by TIMS on a Finnigan MAT-262 spectrometer. The values thus obtained were normalized to $^{88}Sr/^{86}Sr = 8.375209$ and $^{146}Nd/^{144}Nd = 0.7219$. The blanks were 0.6 and 0.09 ng for Sr and Nd, respectively. The accuracy (2σ) was evaluated by ten replicate analyses of the WS-E standard and was no worse than 0.003% for the $^{87}Sr/^{86}Sr$ ratio and 0.0015% for the

Table 2. Chemical composition (wt %) of olivine, orthopyroxene, and clinopyroxene

Component	Olivine			Orthopyroxene		Clinopyroxene						
	PRXpl[1]	GBRol	GBRS	PRXpl	GBRol	PRXpl	GBRol	GBR	GBRS	GRAN	FOID	FOID
	111/275**[2]	51/23	GV-106	111/275	51/23	111/275	51/23**	101/258	GV-106	2703	166/60	166/61
SiO_2	36.87	31.69	29.08	54.37	49.49	52.15	50.31	48.94	47.36	50.32	52.53	53.38
TiO_2	nd	nd	nd	nd	0.02	0.83	0.61	0.22	0.59	0.23	0.25	0.20
Al_2O_3	nd	nd	nd	0.41	0.73	1.98	2.00	0.51	0.78	0.70	4.65	5.06
FeO*	24.64	52.32	66.25	16.89	28.62	6.72	13.37	21.79	25.16	27.92	15.09	14.67
MnO	0.31	0.96	3.09	0.36	0.83	0.15	0.40	1.01	0.93	0.66	0.46	0.45
MgO	37.49	14.27	0.72	27.33	17.80	15.42	13.11	5.19	3.01	0.76	5.10	4.97
CaO	0.02	0.01	0.02	0.19	0.66	20.40	19.24	20.94	20.07	12.68	13.79	13.84
Na_2O	na	na	na	0.01	0.01	1.16	0.40	0.66	0.54	5.82	6.26	6.40
Total	99.33	99.25	99.18	99.56	98.17	98.81	99.44	99.06	98.46	99.09	98.13	98.97
	Cations per 4 oxygen ions			Cations per 6 oxygen ions								
Si	0.980	0.981	0.992	1.979	1.951	1.946	1.916	1.970	1.955	2.054	2.031	2.039
Ti	–	–	–	0.000	0.001	0.023	0.017	0.006	0.017	0.007	0.007	0.006
Al	–	–	–	0.018	0.034	0.087	0.092	0.024	0.038	0.034	0.212	0.228
Fe	0.548	1.354	1.889	0.514	0.944	0.210	0.428	0.733	0.869	0.955	0.488	0.468
Mg	1.485	0.658	0.037	1.482	1.046	0.858	0.747	0.314	0.185	0.047	0.294	0.283
Mn	0.007	0.025	0.089	0.011	0.028	0.005	0.013	0.035	0.033	0.023	0.015	0.014
Ca	0.001	0.000	0.001	0.007	0.028	0.816	0.793	0.902	0.888	0.566	0.571	0.566
Na	–	–	–	0.001	0.001	0.083	0.030	0.052	0.043	0.470	0.469	0.474
Mg#	73.1	32.7	1.9	74.2	52.6	80.4	63.6	30.0	17.6	4.7	37.6	37.6
Ca	–	–	–	0.4	1.4	43.3	40.3	46.3	45.7	36.1	43.0	42.2
Mg	–	–	–	74.0	51.8	45.5	38.0	16.1	9.6	3.0	21.5	21.7
Fe	–	–	–	25.7	46.8	11.1	21.7	37.6	44.7	60.9	35.6	36.1
				En	*En*	*Aug*	*Aug*	*Hd*	*Hd*	*Aug*	*Aeg-Aug*	*Aeg-Aug*

Note: Here and in Tables 3–5, **nd** means not detected, **na** means not analyzed. Here and in Table 3, Mg# = Mg/(Mg + Fe_{tot}); *En*—enstatite, *Hd*—hedenbergite, *Aug*—augite, *Aeg-Aug*—aegirine-augite.
* Here and in Tables 3–5, and 15, all Fe is given as FeO.
** Samples used for model simulations.
[1] Here and in Tables 3 and 4, rock (see Table 1 for symbol explanations).
[2] Here and in Tables 3, 4, and 8–11, sample numbers.

$^{143}Nd/^{144}Nd$ ratio. The values for the $^{87}Rb/^{86}Sr$ and $^{147}Sm/^{144}Nd$ ratios were obtained by ICP-MS accurate to 1.2 and 0.9% by the method described in (Montero and Bea, 1998). The methods of isotopic dating with the use of single zircon grains were described in (Bea et al., 2001).

Minerals were analyzed on a Camebax SX-50 microprobe, with the use of synthetic standards. The accelerating voltage was 20 kV, and the beam current was 15 Ma. The variation coefficients were 1, 2.5, and 5% for analyzed concentrations of 10, 1, and 0.25 wt %, respectively.

PETROGRAPHY AND MINERAL CHEMISTRY

Ultrabasic Series

The series is dominated by peridotites, pyroxenites, gabbro, monzonites, and monzosyenites (Table 1), which compose a stratified intrusive body intersected by younger faults (Fig. 2). Its eastern contact zone exposes the gabbronorites of the chill zone, which grade into the rocks of the intrusion itself. The layering of the body is accentuated by cyclically alternating layers of peridotite, gabbro, and leucogabbro. The cycles are 0.5–3.0 m thick. The ultrabasic complex is subdivided into two parts of somewhat different composi-

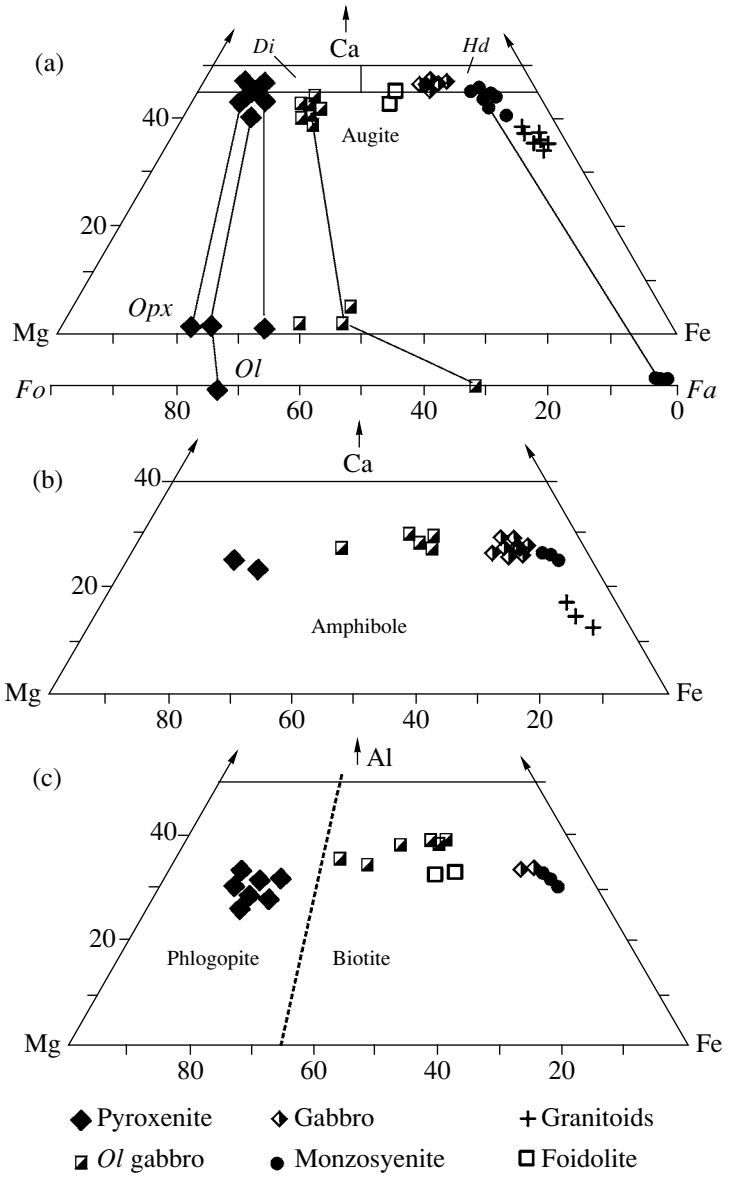

Fig. 3. Composition of minerals from the Gremyakha–Vyrmes Massif.
(a) Ca–Mg–Fe (at %) diagram for the coexisting orthopyroxene and clinopyroxene and forsterite (*Fo*)–fayalite (*Fa*) diagram for the olivine; (b) Ca–Mg–Fe (at %) diagram for the amphibole; (c) Mg–Fe–Al (at %) diagram for the micas.

tion: (i) an eastern part, which consists of cyclically alternating layers of titanomagnetite- and apatite-bearing peridotites and volumetrically subordinate layers of plagioclase-bearing peridotites, troctolites, and olivine gabbro and (ii) a western part, which is made up of predominantly plagioclase-bearing peridotites, pyroxenites, gabbro-diorites, monzonites, and monzosyenites. All rocks of this series are characterized by elevated contents of ilmenite, titanomagnetite, and apatite (Osokin, 1987).

Olivine in the rocks of this complex varies in composition from $Fo_{80–35}$ in the peridotites and pyroxenites to $Fo_{33–5}$ in the gabbro and $Fo_{7–2}$ in the monzosyenites (Table 2). Orthopyroxene of the composition $En_{50–55}$ is contained in the chill-zone gabbronorites in the form of euhedral phenocrysts, often with clinopyroxene rims, in a clinopyroxene–plagioclase–magnetite basis. Orthopyroxene is contained in the main ultrabasic body only in the monzogabbro, in which this mineral composes rims around olivine grains.

Clinopyroxene is present in all of the ultrabasic rocks of the massif, except only its troctolites. This mineral usually occurs as euhedral or subhedral zonal crystals, but the monzonites bear large clinopyroxene oikocrysts with inclusions of euhedral plagioclase grains. The composition of the clinopyroxene is

Table 3. Chemical composition (wt %) of micas and amphiboles

Component	Micas						Amphiboles					
	PRXpl	GBRol	GBR	GBRS	FOID	FOID	PRXpl	GBRol	GBR	GBRS	GRAN	GRAS
	111/275	51/23	101/258	GV-106	166/60	166/61	111/275	51/23	101/258	GV-106	2703	GV-118
SiO_2	40.85	34.26	31.98	33.26	35.92	35.40	42.97	39.04	40.03	39.31	47.02	46.81
TiO_2	0.16	4.83	5.22	6.32	2.27	2.46	0.08	1.99	1.63	1.52	0.77	0.94
Al_2O_3	13.55	14.15	13.02	12.65	12.85	12.76	13.33	13.20	9.47	9.42	2.37	2.44
FeO*	9.57	18.53	30.82	32.73	24.74	25.37	9.43	21.53	29.18	31.61	32.94	32.61
MnO	0.08	0.07	0.27	0.17	0.58	0.60	0.08	0.25	0.66	0.48	0.79	0.88
MgO	22.13	11.10	3.25	2.02	8.50	7.91	15.45	6.33	2.47	1.47	1.53	1.51
CaO	0.05	0.02	0.05	0.02	0.05	nd	10.65	10.65	10.56	10.40	5.11	4.64
Na_2O	0.34	0.10	0.11	0.08	0.17	0.14	3.49	2.12	1.79	1.57	4.51	5.00
K_2O	8.10	8.95	8.24	8.90	9.52	9.50	0.76	1.37	1.32	1.62	1.64	1.73
F	0.31	0.42	0.25	0.42	na	na	0.22	0.21	0.19	0.36	0.77	0.92
Cl	0.03	0.01	0.17	0.12	na	na	0.04	0.07	0.13	0.21	0.04	0.07
SrO	na	na	na	na	0.11	nd	na	na	na	na	na	na
BaO	na	na	na	na	0.84	0.66	na	na	na	na	na	na
Total	94.83	92.02	92.96	96.16	95.55	94.80	96.50	96.76	97.44	97.96	97.49	97.53
	Cations per 22 oxygen ions						Cations per 23 oxygen ions					
Si	5.894	5.433	5.369	5.434	5.707	5.684	6.339	6.133	6.493	6.445	7.682	7.661
Ti	0.018	0.576	0.659	0.776	0.271	0.297	0.009	0.235	0.199	0.187	0.094	0.116
Al	2.304	2.645	2.575	2.434	2.405	2.415	2.319	2.445	1.810	1.820	0.457	0.471
Fe	1.154	2.457	4.325	4.470	3.286	3.405	1.163	2.829	3.959	4.335	4.501	4.463
Mg	4.756	2.622	0.812	0.492	2.012	1.892	3.397	1.481	0.597	0.359	0.372	0.368
Mn	0.010	0.009	0.038	0.024	0.078	0.082	0.010	0.034	0.091	0.067	0.109	0.122
Ca	0.008	0.004	0.008	0.004	0.009	0.002	1.684	1.792	1.836	1.827	0.895	0.814
Na	0.095	0.031	0.035	0.026	0.052	0.044	0.998	0.645	0.562	0.498	1.429	1.586
K	1.491	1.810	1.764	1.853	1.929	1.945	0.143	0.275	0.273	0.339	0.341	0.360
Ba	–	–	–	–	0.143	0.114	–	–	–	–	–	–
Mg#	80.5	51.6	15.8	9.9	38.0	35.7	74.5	34.4	13.1	7.7	7.6	7.6
	Phl	*Bt*	*Bt*	*Bt*	*Bt*	*Bt*	*Prg*	Fe-*Prg*	Fe-*Prg*	Fe-*Prg*	Fe-*Rich*	Fe-*Rich*

Note: *Phl*—phlogopite, *Bt*—biotite, *Prg*—pargasite, Fe-*Prg*—ferropargasite, Fe-*Rich*—ferrorichterite.

Table 4. Chemical composition (wt %) of feldspars

Component	PRXpl	GBR	GBRol		GBRS					GRAN			GRAS
	111/275	101/258	51/23		GV-106					2703			2609
	core	core	core*	margin	core	margin	core	core	core	core	margin	core	core
SiO_2	63.01	65.42	57.38	57.09	61.94	64.72	65.13	63.76	66.51	67.64	68.22	63.06	62.79
TiO_2	0.13	0.01	0.08	0.09	nd	0.04	0.01	0.08	0.01	0.01	nd	0.02	0.17
Al_2O_3	22.42	21.49	26.06	26.03	19.21	20.09	20.46	18.91	19.92	19.32	19.32	18.04	22.72
FeO*	0.13	0.04	0.08	0.11	0.21	0.06	0.03	0.08	0.10	0.22	0.05	0.13	0.16
CaO	3.35	2.46	7.93	8.00	4.56	1.11	1.44	0.32	0.70	0.01	nd	nd	3.67
Na_2O	9.43	10.41	6.94	6.96	10.50	8.96	11.06	4.14	9.55	11.81	11.89	0.34	9.37
K_2O	0.12	0.14	0.28	0.26	0.07	3.43	0.07	10.20	2.87	0.14	0.07	16.49	0.19
Total	98.59	99.96	98.75	98.54	96.49	98.40	98.21	97.49	99.66	99.16	99.54	98.08	99.07
Si	2.820	2.881	2.602	2.596	2.862	2.923	2.914	2.966	2.953	2.986	2.995	2.985	2.802
Ti	0.004	0.000	0.003	0.003	0.000	0.001	0.000	0.002	0.000	0.000	0.000	0.001	0.006
Al	1.183	1.115	1.393	1.395	1.046	1.070	1.079	1.037	1.043	1.006	1.000	1.006	1.195
Fe	0.004	0.002	0.003	0.004	0.008	0.002	0.001	0.003	0.004	0.008	0.002	0.005	0.006
Ca	0.160	0.116	0.385	0.390	0.226	0.054	0.069	0.016	0.033	0.000	0.000	0.000	0.175
Na	0.818	0.888	0.610	0.614	0.940	0.784	0.960	0.374	0.822	1.011	1.012	0.031	0.811
K	0.007	0.008	0.016	0.015	0.004	0.198	0.004	0.605	0.162	0.008	0.004	0.996	0.011
Ab	83.0	87.7	60.3	60.2	80.3	75.7	92.9	37.5	80.8	99.2	96.6	3.1	81.3
An	16.3	11.5	38.1	38.2	19.3	5.2	6.7	1.6	3.3	0.0	0.0	0.0	17.6
Or	0.7	0.8	1.6	1.6	0.4	19.1	0.4	60.8	16.0	0.8	0.4	96.9	1.1

Notes: * Sample used for the model simulations.

strongly correlated with the composition of the rocks: diopside is contained in the peridotites and pyroxenites, augite is present in the olivine-bearing gabbro, and hedenbergite was found in the monzonites and monzosyenites (Table 2, Fig. 3).

Amphibole occurs as a minor mineral, commonly in association with clinopyroxene and partly replaces it. The rocks with elevated amphibole contents are prone to be spatially restricted to the zones of younger tectonization. The amphibole inherits its composition from the replaced clinopyroxene: the pyroxenites contain magnesian pargasite, and the monzonites and monzosyenites bear feropargasite (Table 3, Fig. 3).

Mica is widespread in the peridotites and gabbro in the form of aggregates that partly or completely replace pyroxenes and amphiboles. The composition of the mica varies from phlogopite in the peridotites to biotite in the gabbro and monzosyenites (Table 3, Fig. 3).

Plagioclase in the rocks of the ultrabasic series broadly varies in composition and morphology. Sporadic anhedral plagioclase microlites in the peridotites and pyroxenites have the composition $An_{65–45}$. The gabbro contains morphologically variable plagioclase grains, from euhedral to anhedral, often zonal, whose composition ranges from $An_{51–35}$ in the cores to $An_{26–11}$ in the rims of grains (Table 4). The monzogabbro and monzonites contain large plagioclase laths, varying from $An_{40–25}$ to $An_{20–10}$ in composition, with poikilitic clinopyroxene inclusions. The monzosyenites bear zonal oligoclase–albite grains in association with orthoclase ($An_2Ab_{38}Or_{60}$), which compose complicated textures of mutual replacement.

The apatite contents in some layers of the magnetite and ilmenite cumulates of the ultrabasic series reach 20 vol %. The magmatic apatite occurs in two generations: small euhedral crystals in the peridotites, gabbro, and monzonites and anhedral grains in the apatite–ilmenite–magnetite cumulates. According to Osokin (1987), the concentrations of SrO and the sum of REE in the apatite vary within the ranges of 0.16–0.46 and 0.19–0.45 wt %, respectively. In addition to apatite, ilmenite, and magnetite, the rocks contain accessory zircon and barite.

Granitoid Series

The granitoids occur in the northern part of the massif, in which they form a zonal oval body 12 × 6 km of leucocratic syenogranites in its marginal zone and quartz syenites in the core. The rocks of the complex have a weak gneissosity, which is spatially related to fault zones of northwestern and northeastern trend. The same faults in the granitoids are accompanied by segregations of coarse-grained amphibole and quartz–feldspar and quartz–amphibole veins with zircon and allanite.

The granitoids are dominated by alkali-feldspar granites, monzogranites, and quartz syenites, which contain, along with major minerals, also zonal aegirine-augite, arfvedsonite (which partly or completely replaces this pyroxene), richterite, and aenigmatite. Analyses of the minerals are presented in Tables 2–4. The feldspars are euhedral laths of primary oligoclase ($An_{18}Ab_{81}Or_1$) and orthoclase, which are sometimes replaced by secondary albite and microcline. The accessories are apatite, ilmenite, aenigmatite, titanite, zircon, monazite, and barite. A Ti–LREE–Ca phase (perhaps, primary knopite) and secondary LREE–Ca carbonate rich in Sr (perhaps, khanneshite) were identified under an electron microscope.

Foidolite Series

The rocks of this series compose a number of fragments of a single body 2 × 5 km in size in the central part of the massif, among ultrabasites and granitoids. The fenitized gabbro and syenogranite zones, which were described earlier near the northern contact of the massif (Kukharenko et al., 1971; Vinogradov et al., 1985), and small ijolite and nepheline syenite dikes and veins suggest that the foidolite series corresponded to the final evolutionary stage of the Gremyakha–Vyrmes Massif.

The foidolites of the largest blocks exposed at the surface display layering in the form of layers of melteigite and ijolite unsystematically alternating with layers of juvite and nepheline syenite. The foyaites, which vary in composition from agpaitic to miaskitic varieties, develop as a network of large veins that cut across the foidolites. Clinopyroxene, the main mafic mineral of the foidolites, varies in composition from aegirine-augite in the melteigites and ijolites to aegirine in the juvites and nepheline syenites (Table 2). Clinopyroxene in these rocks is characterized by elevated concentrations of the tschermakite end member (8–11 mol %). The amphibole (hastingsite) is relatively rare and occurs mostly as aggregates with clinopyroxene. The micas of the foidolites and nepheline syenites are biotite, which replaces other mafic minerals. The accessory minerals are Mn-rich ilmenite, titanite, apatite, zircon, baddeleyite, Ti–Fe–Ba silicate (perhaps, benitoite), barite, and celestite. The only REE-bearing phase, which was identified by SEM, is metamict, Ca-poor allanite. In contrast to their analogues in the ultrabasic series of the massif, apatite and titanite in the foidolites are notably enriched in SrO and REE (Table 5).

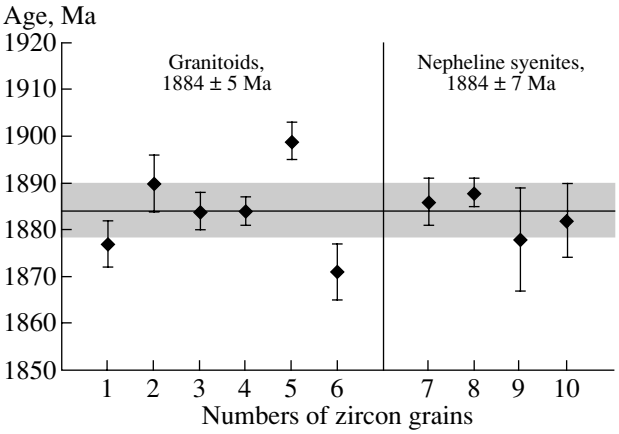

Fig. 4. Data of the isotopic dating of single zircon grains from granitoids and nepheline syenites of the Gremyakha–Vyrmes Massif.

The youngest phase of the massif consists of thin carbonate veins, which display, according the latest isotopic geochemical data (Savatenkov et al., 1999), evidence of affiliation with carbonatites. Similar rocks in fault zones were previously regarded as young hydrothermal veins related to regional metamorphic processes (Polkanov et al., 1967).

In addition to these rocks, the massif contains much nepheline-bearing syenites (pulaskites), monzosyenites (ankerites), laurdalites, and heterogeneous rocks of composition intermediate between those of the syenites, monzonites, foidolites, and gabbro. Considering the spatial restriction of these rocks to the marginal zones and contacts of the complexes, it seems to be reasonable to relate their genesis to contact metasomatic processes.

GEOCHRONOLOGY

Available geochronologic dates on the Gremyakha–Vyrmes Massif (which were obtained by different methods for distinct rock complexes) are significantly scattered. The U–Pb zircon and titanite ages of monzogabbro from the ultrabasic series are equal to

Table 5. Representative analyses (wt %) of minerals from the foidolite series

Component	Nepheline		Sodalite	Apatite		Titanite		
	166/60	166/61	166/60	166/60	166/61	166/60	166/61	166/62
SiO_2	42.12	42.65	37.16	0.48	0.38	30.18	30.30	30.28
TiO_2	nd	0.03	0.14	0.08	0.04	37.85	37.29	37.04
Al_2O_3	33.91	33.62	31.65	na	na	0.60	1.04	1.03
FeO	0.05	0.09	0.07	nd	nd	0.88	1.12	1.00
MnO	na	na	na	0.03	nd	0.03	nd	nd
CaO	0.06	0.05	0.29	52.27	52.41	27.42	27.62	27.65
Na_2O	16.73	16.42	23.57	nd	0.15	0.22	0.25	0.18
K_2O	6.19	6.33	nd	nd	0.03	na	na	na
P_2O_5	na	na	na	40.60	41.44	0.19	0.15	0.16
Cl	na	na	6.97	na	na	na	na	na
SrO	na	na	na	1.69	1.46	0.31	0.22	0.20
ZrO_2	na	na	na	na	na	1.20	1.07	0.93
La_2O_3	na	na	na	0.21	0.15	0.12	0.06	0.08
Ce_2O_3	na	na	na	0.57	0.36	0.36	0.17	0.28
Nd_2O_3	na	na	na	0.27	0.18	0.18	0.17	0.15
Total	99.06	99.19	99.85	96.20	96.60	99.54	99.46	98.98

Table 6. Kober zircon ages of rocks from the massif

Zircon grain	Rock	$^{204}Pb/^{206}Pb$	$^{207}Pb/^{206}Pb$	$^{204}Pb/^{206}Pb$ (corrected)	Error (2σ)	Age, Ma
1	Syenogranite	0.000643	0.123233	0.114835	0.28	1877 ± 5
2	Syenogranite	0.000647	0.124358	0.115645	0.34	1890 ± 6
3	Syenogranite	0.000658	0.124127	0.115269	0.21	1884 ± 4
4	Syenogranite	0.000658	0.124115	0.11525	0.13	1884 ± 3
5	Syenogranite	0.000646	0.124908	0.116216	0.22	1899 ± 4
6	Syenogranite	0.000355	0.118926	0.114416	0.29	1871 ± 6
7	Nepheline syenite	0.000653	0.123944	0.115420	0.29	1886 ± 5
8	Nepheline syenite	0.000242	0.118530	0.116373	0.16	1888 ± 3
9	Nepheline syenite	0.000397	0.119959	0.114885	0.59	1878 ± 11
10	Nepheline syenite	0.000662	0.123763	0.115119	0.41	1882 ± 8

1973 ± 5 Ma (Vursii et al., 2000), and a Pb–Pb isochron for apatite from the gabbro and peridotite corresponds to an age of 1911 ± 87 Ma (Savatenkov et al., 1998). The Sm–Nd isochron age of the basites is 1926 ± 74 Ma (Savatenkov et al., 1998), which roughly corresponds to the first approximate K–Ar dates for the massif (Kukharenko et al., 1971). The youngest ages of the hyperbasites (1865 ± 100 Ma) were obtained by the Pb–Pb method on apatite from alkali gabbro (Pushkarev, 1990). At the same time, the ages of carbonatite veins that cut the rocks of the Gremyakha–Vyrmes Massif and are obviously younger than the rocks of the ultrabasic series are equal to 1945 ± 4 Ma (zircon, U–Pb method) and 2034 ± 46 Ma (Sm–Nd method) (Savatenkov et al., 1999). The dating of the syenites by independent methods yielded an age of 1872 ± 8 Ma (Bea et al., 2001), which coincides with the age of the analogous rocks in the Soustova Massif. These data suggest that the reason for the scatter of the dates of the oldest ultrabasic complex was the multiple distortion of the isotopic systems related to the thermal and chemical influence of acid and alkaline magmas (that produced the granitoid and foidolite series of the Gremyakha–Vyrmes Massif) on the gabbro and peridotites and to the younger alterations of all rocks by regional metamorphism.

With regard for the data presented above, the task of our geochronological research was formulated as the dating of, first of all, the granitoids and foidolites. The method based on stepwise Pb evaporation from single zircon grains from the alkaline granitoids (seven grains) and nepheline syenites (four grains) yielded average ages of 1884 ± 5 and 1884 ± 7 Ma, respectively (Table 6, Fig. 4). A mineral isochron obtained for the foidolites corresponds to an age of 1892 ± 9 Ma ($(^{87}Sr/^{86}Sr)_0$ = 0.70232, Fig. 5a), which is consistent with the rough estimate made by Kukharenko et al. (1971) by the Th–U–Pb method on pyrochlore from aegirinite. To date the ultrabasites and granitoids, we calculated a regression equation for all Rb–Sr dates obtained from the rocks of the two complexes (Table 7). We failed, however, to obtain a satisfactory age estimate. Taking into account the possibility that the isotopic systems could be distorted under the effect of younger alkaline melts, we constructed an isochron that did not involve data on the varieties of the gabbroids affected by alkaline metasomatism (monzosyenites and pulaskites). The resultant regression equation for the Rb–Sr dates of the rocks of the ultrabasic and granitoid series corresponds to an age of 1881 ± 16 Ma at $(^{87}Sr/^{86}Sr)_0$ = 0.70382 (Fig. 5b). Our data suggest that the ultrabasic, granitoid, and alkaline series of the massif were produced within a relatively narrow age interval of 1885 ± 20 Ma.

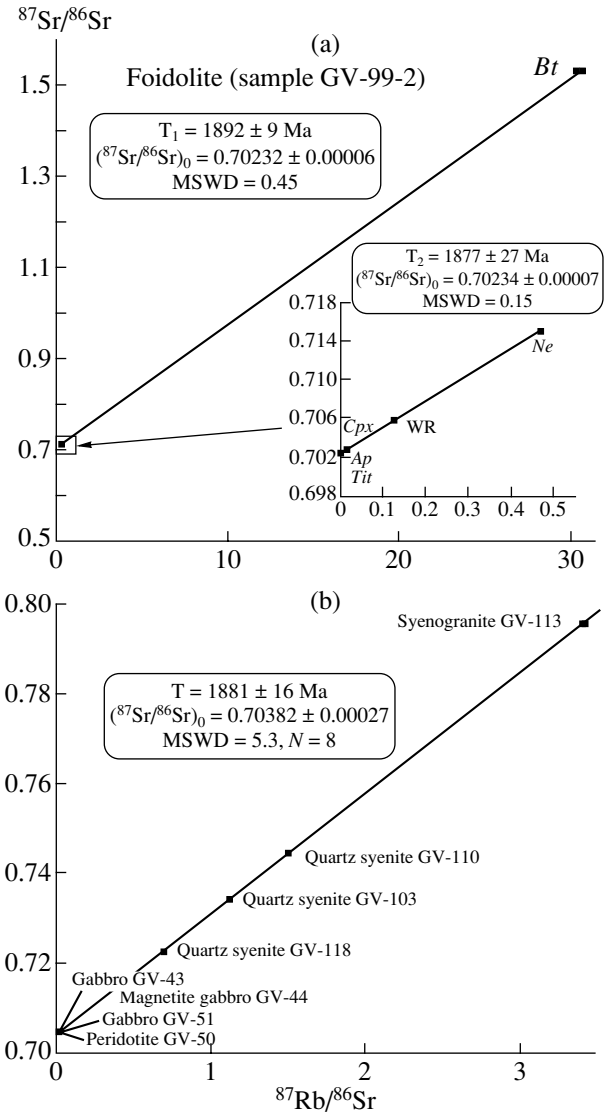

Fig. 5. Rb–Sr isochron diagram for (a) foidolite and (b) rocks of the ultrabasic and granitoid series of the Gremyakha–Vyrmes Massif.

Diagram in Fig. 5a presents the ages calculated for all points (T_1) and those without biotite (T_2). Errors along the $^{87}Rb/^{86}Sr$ and $^{87}Sr/^{86}Sr$ axes are 1.2 and 0.002% (2σ), respectively. *Bt*—biotite, *Ne*—nepheline, WR—whole rock, *Cpx*—clinopyroxene, *Ap*—apatite, *Tit*—titanite.

GEOCHEMISTRY

Major Elements

Among the Proterozoic rocks of northeastern Fennoscandia, the rock series of the Gremyakha–Vyrmes Massif are the most alkaline. In the TAS diagram (Fig. 6), these series plot within the field of rocks of elevated alkalinity and define three discrete petrochemical series. The Harker diagram (Fig. 7) demonstrates distinct evolutionary trends for each of the series, which imply that these series could be produced by different parental melts. The ultrabasic series is characterized by

Table 7. Rb–Sr isotopic data on rocks and minerals from the Gremyakha–Vyrmes Massif

Rock	Sample	Rb, ppm	Sr, ppm	$^{87}Rb/^{86}Sr$	$^{87}Sr/^{86}Sr$	$(^{87}Sr/^{86}Sr)_{(T)}$	ε_{Sr}
Peridotite	GV-50*	4.20	783	0.016	0.704311	0.703878	23.0
Gabbro	GV-51*	4.29	841	0.015	0.704345	0.703939	23.9
Gabbro	GV-43*	10.4	976	0.031	0.704752	0.703913	23.5
Magnetite gabbro	GV-44*	0.143	16.1	0.026	0.704558	0.703855	22.7
Monzosyenite	GV-106	23.7	103	0.667	0.723143	0.705097	40.4
Pulaskite	GV-104	79.7	266	0.867	0.725758	0.702301	0.5
Pulaskite	GV-109	116	221	1.518	0.744699	0.703629	19.5
Syenogranite	GV-113*	76.0	65.3	3.396	0.796050	0.703169	27.2
Quartz syenite	GV-110*	84.9	164	1.504	0.744119	0.703427	16.6
Quartz syenite	GV-118*	59.1	247	0.693	0.722267	0.703518	17.9
Quartz syenite	GV-103*	76.3	198	1.118	0.734294	0.705246	25.4
Ijolite	GV-100	35.2	965	0.105	0.709528	0.706687	63.0
Ijolite	GV-1/9A	49.7	811	0.177	0.707162	0.702373	1.6
Laurdalite	GV-111	89.9	1239	0.210	0.708997	0.703315	15.0
Nepheline syenite	GV-1/2	80.9	754	0.311	0.712491	0.704077	25.8
Ijolite, whole rock	GV-99-2*	45.2	1030	0.1269	0.705776	0.702342	1.1
Ijolite, apatite	GV-99-2*	0.22	7991	0.0001	0.702373	0.702371	–
Ijolite, titanite	GV-99-2*	0.45	1482	0.0009	0.702373	0.702349	–
Ijolite, pyroxene	GV-99-2*	1.78	319	0.0161	0.702741	0.702304	–
Ijolite, nepheline	GV-99-2*	54.2	354	0.4438	0.714334	0.702327	–
Ijolite, biotite	GV-99-2*	426	43.8	30.462	1.532823	0.708669	–

Note: The $(^{87}Sr/^{86}Sr)_T$ and ε_{Sr} values were calculated for an age of 1880 Ma.
* Data used for the isochron calculation.

the presence of normative nepheline in its rocks, including their most silicic varieties. More mafic varieties of the ultrabasites are anomalously enriched in Fe_2O_{3tot}, TiO_2, and P_2O_5. In the diagrams of Fig. 7, the rocks of the series define a clearly pronounced trend suggesting that these rocks were formed by the successive crystallization of olivine, ortho- and clinopyroxene, plagioclase, titanomagnetite + ilmenite, and apatite from the melt, with the crystallization of the latter proceeding concurrently with the settling of olivine and pyroxene. The leucocratic varieties of this series include hybrid rocks enriched in K_2O. All rocks of the series display direct correlations between their Na_2O and K_2O concentrations. Representative analyses of rocks of this series are listed in Table 8.

The high alkalinity of the rocks of the granitoid series is obvious from the fact that they contain 1–3% normative acmite and also from the values of their agpaitic coefficient $K_{agp} = (Na_2O + K_2O)/Al_2O_3 = 1.02–1.11$. In the diagram of Fig. 7, the data points of the rocks define a trend with a systematic enrichment in alkalis and alumina. In contrast to the ultrabasites, the granitoids exhibit no direct correlation between the contents of Na_2O and K_2O.

The rocks of the foidolite series are characterized by fairly significant variations in the concentrations of most major oxides at relatively insignificant variations in the silica content (Fig. 7). The concentrations of normative acmite in these rocks exceed 5 mol %, and the $(Na_2O + K_2O)/Al_2O_3$ ratios of the ijolites and melteig-

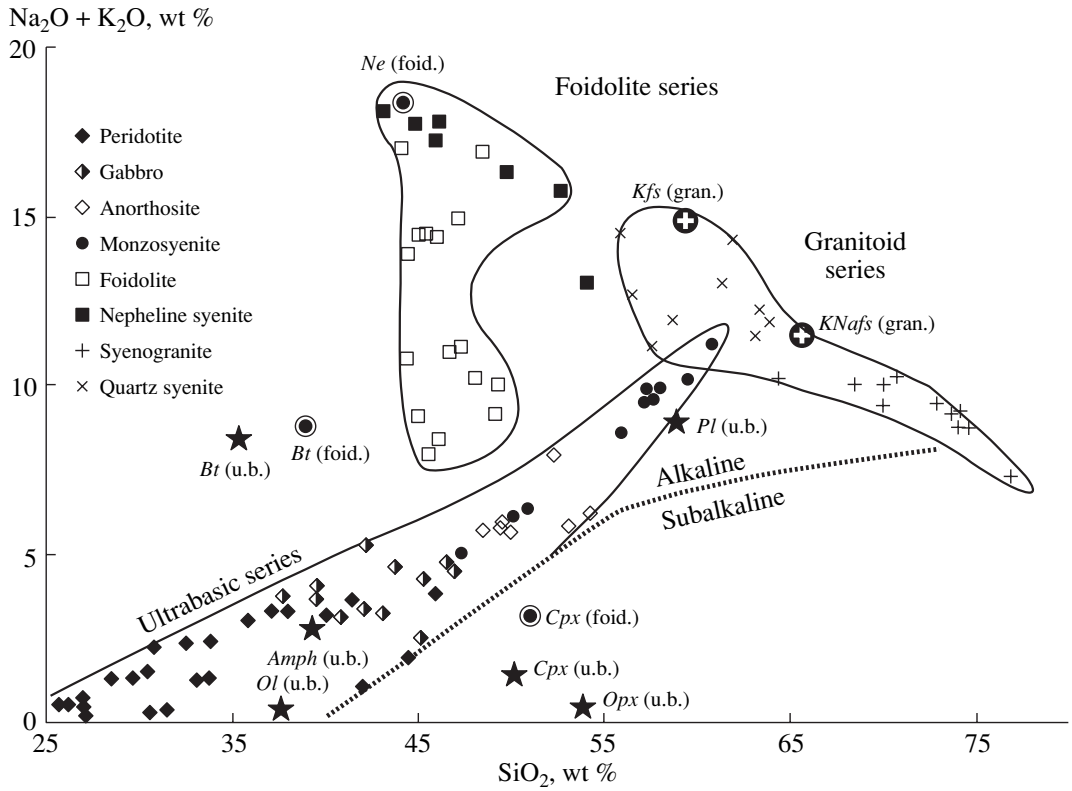

Fig. 6. ($Na_2O + K_2O$) vs. SiO_2 diagram for rocks of the Gremyakha–Vyrmes Massif. The diagram displays the composition of minerals from the ultrabasic (u.b.), granitoid (gran.), and foidite (foid.) series.

ites are equal to 1.01–1.14. At the same time, the K_{agp} of the nepheline syenites varies from 0.85 to 1.01 and suggests that these rocks mostly belong to the miaskitic series. Representative analyses of rocks of the granitoid and foidolite series are listed in Table 9.

Trace Elements

The concentrations of trace elements in representative samples of rocks from the massif are presented in Tables 10 and 11.

The Ni concentrations in the rocks of the ultrabasic series are lower than in the ultrabasites, including the ultrabasic rocks of the Pechenga Group (Smolkin, 1992). The contents of Co, Sc, and V in the rocks are directly correlated with MgO, which suggests that the ultrabasic melt evolved under olivine, clinopyroxene, and titanomagnetite control (Fig. 8). Judging from the absence of a clear correlation between Ni and MgO, Ni-bearing magnesian olivine played a determining role only early in the course of melt evolution, and the mineral predominantly crystallizing in the chamber was fayalite. The fractionation of trace elements in the peridotites, gabbro, and altered rocks of the series (monzosyenites) is similar (Fig. 9). All basites are characterized by elevated concentrations of Ba, LREE, P, and Ti and significant negative K, Sr, Zr, and Hf anomalies. The REE patterns of the rocks (Fig. 10) are characterized by high concentrations of LREE, 150 times higher than the chondritic values, and their weak fractionation, $(La/Sm)_N$ = 1.26–1.57. The concentrations of MREE and HREE gradually decrease to values ten times higher than the chondritic values for Yb and Lu. The positive Eu anomaly (Eu/Eu*) clearly pronounced in the rocks of the complex gradually increases from 1.32–1.48 in the peridotites to 1.47–1.72 in the gabbro and reaches a maximum of ~6.4 in the monzosyenites.

The rocks of the granitoid series display features suggesting their complementary character with the rocks of the ultrabasic series. In trace-element plots (Fig. 9), the syenogranites and quartz syenites have clearly pronounced negative Sr, P, Ti, and Ba (in the syenogranites) anomalies, which correspond to the positive anomalies of these elements in the peridotites and gabbro. The pulaskites, which are, in fact, the marginal facies of the granitoid series near the foidolites, show similarities with both the nepheline syenites and the quartz syenites. The syenogranites are the only rocks of the massif with negative Eu anomalies (Eu/Eu* = 0.51–0.60).

The rocks of the foidolite series display no geochemical similarities with the rocks described above and are characterized by extremely broad variations in the concentrations of most trace elements. This is explained by the fact that these rocks contain rare accessories concentrating Th, U, Zr, Hf, Nb, Ta, and

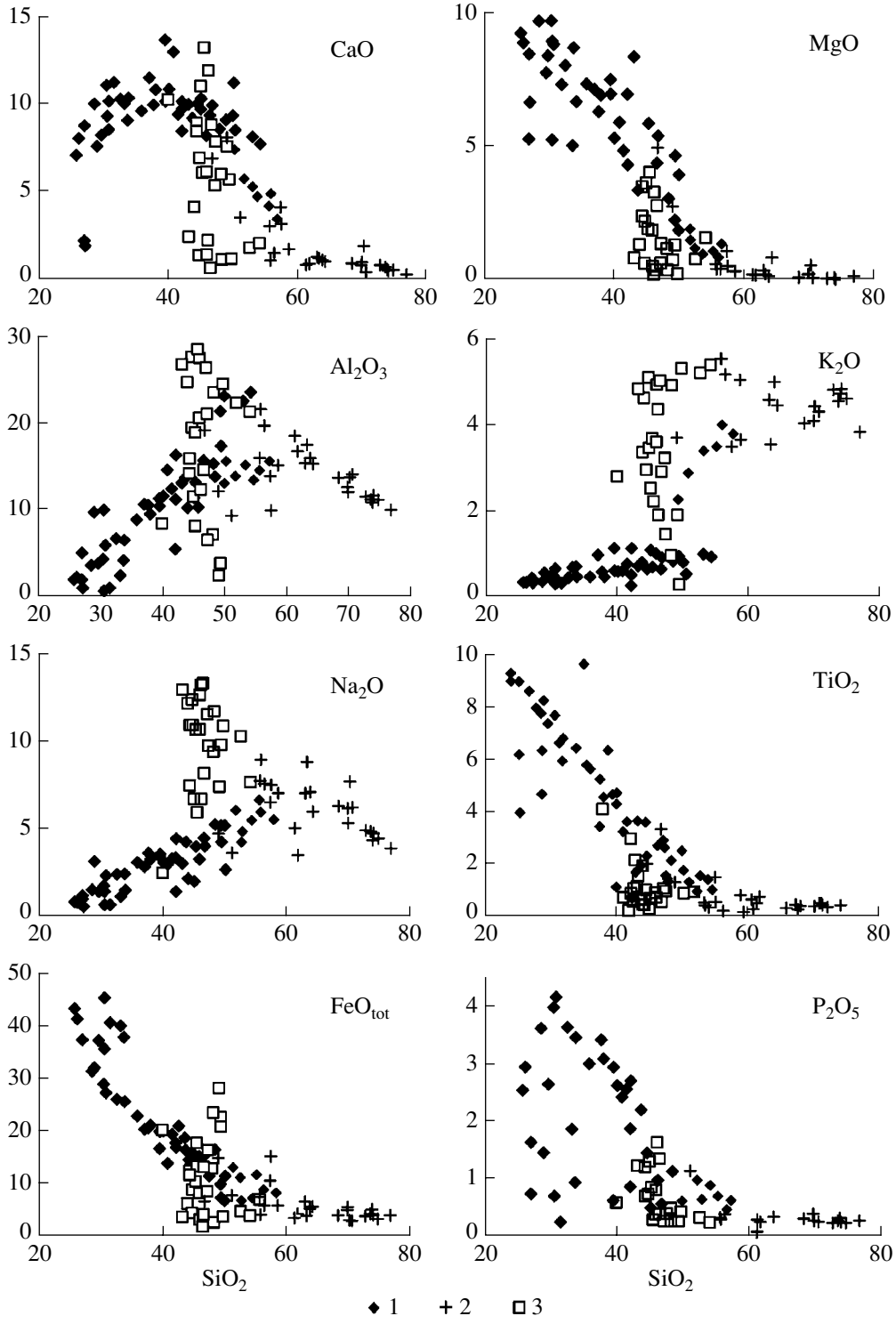

Fig. 7. Oxide–SiO_2 (wt %) diagrams for rocks of the Gremyakha–Vyrmes Massif.
(1) Ultrabasic series; (2) granitoid series; (3) foidolite series. The diagram was constructed with the use of data from (Polkanov et al., 1967; Kukharenko et al., 1971; Vinogradov et al., 1985).

other elements. For example, aegirinite (Table 10, sample GV-114) from the Egirinovyi Navolok area contains much pyrochlore and zircon. The REE patterns of the foidolites in Fig. 10 typically have a S-shaped bend and display certain similarities with the REE patterns of the laurdalites (alkalized contact varieties of the gabbro series). The foidolites have concentrations of most trace elements close to those in the analogous rocks of Pale-

Table 8. Representative chemical analyses (wt %) of rocks from the layered gabbro–peridotite series

Component	Peridotite						*Ol* gabbro	Gabbro
	GV-19	GV-20	GV-46	GV-49	GV-50	GV-52	GV-22	GV-15
SiO_2	33.38	30.47	30.86	28.61	35.90	32.61	38.07	38.07
TiO_2	6.52	7.55	8.03	8.38	6.26	7.48	5.48	5.10
Al_2O_3	6.73	4.54	6.13	3.82	9.09	6.93	9.75	10.68
$Fe_2O_3^*$	28.11	30.25	29.46	34.11	25.59	29.11	22.65	22.02
MnO	0.33	0.35	0.33	0.37	0.29	0.31	0.27	0.26
MgO	8.66	9.67	8.79	9.66	7.32	8.00	6.89	6.94
CaO	10.47	11.20	10.28	10.13	9.73	10.41	10.95	10.27
Na_2O	2.08	1.35	1.97	1.11	2.77	2.04	2.97	3.26
K_2O	0.25	0.11	0.18	0.14	0.25	0.23	0.25	0.40
P_2O_5	3.39	3.94	4.13	3.56	2.91	3.58	3.00	2.85
LOI	0.97	0.77	0.55	0.44	0.20	0.28	0.33	0.89
Total	100.89	100.20	100.71	100.33	100.31	100.98	100.61	100.74

Component	Gabbro					Monzosyenite		
	GV-43**	GV-45	GV-51	GV-64	GV-44***	GV-105	GV-115	GV-106
SiO_2	45.37	46.65	42.12	37.52	28.99	60.86	59.23	57.53
TiO_2	3.54	3.49	4.17	5.45	12.72	0.52	1.08	1.02
Al_2O_3	13.41	15.95	11.45	10.76	9.97	17.40	16.05	15.62
$Fe_2O_3^*$	15.61	14.25	19.91	23.08	33.78	5.32	9.85	9.55
MnO	0.20	0.16	0.24	0.27	0.28	0.11	0.24	0.28
MgO	5.84	4.36	6.93	6.28	3.79	0.22	0.45	0.52
CaO	10.41	8.52	10.27	10.08	6.79	2.53	3.21	2.73
Na_2O	3.73	4.23	3.04	3.32	2.82	6.87	6.13	6.10
K_2O	0.49	0.44	0.30	0.37	0.35	4.40	3.95	3.88
P_2O_5	1.20	0.64	1.73	3.35	1.29	0.19	0.27	0.22
LOI	0.19	0.80	0.37	0.47	0.17	0.89	0.11	1.54
Total	99.99	99.49	100.53	100.95	100.95	99.31	100.57	98.99

Note: * Here and in Tables 9 and 13, all Fe is given in the form of Fe_2O_3.
** Sample used for the model simulations.
*** GV-44—magnetite-bearing gabbro.

ozoic alkaline intrusions in the province (the only exceptions are the higher LREE concentrations in the Paleozoic varieties). The concentrations of trace elements in a typical foidolite sample from the Gremyakha–Vyrmes Massif and in its minerals are presented in Fig. 11. It can be seen that the REE patterns of the ijolite are mostly controlled by clinopyroxene and, to a lesser degree, apatite and titanite, whereas the nepheline and biotite control is very weak.

Sr AND Nd ISOTOPIC SYSTEMATICS

The Sr isotopic composition of rock samples from all series of the massif are similar and vary within

Table 9. Representative chemical analyses (wt %) of rocks from the granitoid and foidolite series

Component	Syenogranite		*Qtz* syenite				Pulaskite		Ijolite		Aegirinite	Nepheline syenite		Laurdalite	Gneiss ***
	GV-117	GV-113	GV-102	GV-103	GV-110	GV-118	GV-104	GV-109	GV-1/9-A	GV-100	GV-114*	GV-107	GV-1/2**	GV-111	4**
SiO_2	76.78	70.56	73.89	69.80	63.79	68.35	55.80	56.39	44.39	47.20	49.40	46.15	52.58	55.68	64.22
TiO_2	0.40	0.37	0.41	0.42	0.48	0.30	0.40	0.32	0.84	0.26	1.02	0.43	0.85	0.50	0.26
Al_2O_3	10.24	14.33	11.89	12.86	16.22	13.96	21.90	19.98	16.17	21.34	4.05	28.03	22.75	16.24	20.17
Fe_2O_3	4.66	3.47	4.68	5.06	6.05	4.61	3.98	5.68	13.13	9.69	22.38	3.70	5.50	7.39	2.24
MnO	0.08	0.09	0.09	0.09	0.13	0.10	0.10	0.14	0.23	0.25	0.42	0.04	0.09	0.17	0.02
MgO	0.13	0.08	0.01	0.20	0.13	0.09	0.40	0.41	2.38	0.62	1.30	0.13	0.77	0.59	0.58
CaO	0.31	0.46	0.53	0.86	1.16	0.94	1.12	1.56	8.56	5.45	5.79	2.28	1.87	3.10	3.12
Na_2O	3.60	6.09	4.52	6.02	7.03	6.16	8.97	7.51	11.07	11.72	9.87	13.50	10.39	7.70	7.82
K_2O	3.76	4.25	4.80	4.03	4.97	3.97	5.53	5.15	2.84	3.13	0.07	4.31	5.19	5.54	1.49
P_2O_5	0.05	0.03	0.03	0.18	0.12	0.09	0.08	0.11	0.50	0.04	0.04	1.48	0.11	0.11	0.08
LOI	0.07	0.09	0.08	0.46	0.17	0.54	1.35	1.95	0.20	0.87	0.65	0.45	0.32	2.56	–
Total	100.08	99.82	100.93	99.98	100.25	99.11	99.63	99.20	100.31	100.57	94.99	100.50	100.42	99.58	100.00

Note: * GV-114—pyrochlore-bearing aegirinite.
** Samples used for the model simulations.
*** Composition of Archean plagioclase gneiss (Vetrin et al., 1999).

0.70390 ± 0.00004, 0.70421 ± 0.00105, and 0.70384 ± 0.00005 for the ultrabasites, granitoids, and foidolites, respectively. Since the $(^{87}Sr/^{86}Sr)_{T = 1880\ Ma}$ of the host gneisses is 0.7166 (Savatenkov et al., 1998), it is reasonable to hypothesize that the participation of crustal material in the origin of the rocks was at a minimum. The calculation of isotopic mixing models indicates that the percentage of crustal material in the rocks of the series does not exceed 10%. Some rocks of the massif, which occur locally, such as the monzosyenites, pulaskites, laurdalites, and pegmatoid foidolites (sample GV-100), show a broad scatter of their Sr and Nd isotopic ratios, a feature possibly pointing to a hybrid origin of these rocks. The Nd isotopic composition of the rocks broadly varies and makes it possible to reveal significant differences in the composition of the complexes (Table 12). In a $^{87}Sr/^{86}Sr$–ε_{Nd} diagram (Fig. 12), the highest ε_{Nd} values are typical of the foidolites; the gabbro, peridotites, pulaskites, and granitoids define a trend whose continuation passes through the data points of granitoids from the Litsa–Ara Guba Complex and its host basement gneisses. The model ages, calculated with respect to the depleted mantle, significantly vary and are much older than the isotopic dates obtained by different methods (Table 12). To minimize the effect of the crustal complex, the model ages T(DM) were calculated following the procedure described in (Liew and Hofmann, 1988). The calculations yielded quite close age values for the rocks of the ultrabasic series and granitoids (2470 ± 145 Ma) and younger ages for the foidolites (2340 ± 110 Ma).

GENESIS OF THE MASSIF

Parental Magmas

According to isotopic dates, the Gremyakha–Vyrmes Massif was formed during the final evolutionary stage of the Pechenga–Varzuga rift zone. This led to the idea that the parental magmas of the massif were generated during the pulse of endogenic activity that also brought about the ultrabasic melts of the Pechenga structure (Sharkov and Smolkin, 1998).

Ultrabasic series. The weighted mean composition of the series, calculated with regard for the volumes of all rock varieties, is close to the composition of the gabbro (sample GV-43). Inasmuch as the main eruptions of ferropicritic melts occurred in the Pechenga structure at 1990 ± 40 Ma (Smolkin, 1992) and continued until the closure of the rift structure at 1.85–1.75 Ga, the parental magmas of the ultrabasic series of the Gremyakha–Vyrmes Massif could correspond to the most primitive ultrabasic volcanics in the fourth Pechenga volcano-

Table 10. Concentrations of trace elements (ppm) in rocks from the layered gabbro–peridotite series

Element	Peridotite				*Ol* gabbro	Gabbro						Monzosyenite		
	GV-19	GV-20	GV-50	GV-52	GV-22	GV-15	GV-43	GV-45	GV-51	GV-64	GV-44	GV-105	GV-115	GV-106
Li	5.00	3.44	3.10	5.17	3.24	6.71	6.74	3.72	5.44	3.31	0.75	3.19	4.91	7.07
Rb	6.51	3.03	3.91	5.51	3.41	12.5	11.5	6.67	4.70	8.33	1.29	14.81	16.51	23.17
Cs	0.26	0.16	0.17	0.59	0.14	0.57	0.59	0.35	0.22	0.44	0.01	0.25	0.20	0.45
Sr	616	437	783	606	838	912	976	724	841	971	16.1	129	114	107
Ba	307	178	439	280	441	514	497	381	474	550	6.63	11960	6899	6871
Sc	28.9	34.1	22.1	23.2	28.6	24.3	22.1	16.2	25.1	17.8	3.43	10.0	14.3	10.0
V	285	332	252	320	210	189	171	712	213	183	94.2	0.5	0.7	1.8
Cr	15.5	13.6	34.2	77.5	20.9	29.8	67.2	50.7	148	23.7	2213	9.9	10.4	7.1
Co	64.7	74.2	57.0	67.7	48.8	45.6	38.1	70.4	46.1	46.2	85.5	1.1	2.4	3.1
Ni	7.2	7.7	13.2	33.2	8.2	9.2	30.8	17.5	60.7	7.8	2206	4.8	6.2	6.4
Cu	42.5	48.1	38.4	57.4	36.3	35.7	34.6	62.4	33.2	36.1	13.3	5.8	8.2	13.3
Zn	168	260	149	174	133	125	87.4	205	127	142	180	211	201	246
Y	27.1	29.0	22.9	27.2	23.6	24.0	13.5	11.5	16.6	28.7	0.5	4.7	5.8	7.2
Nb	19.6	13.1	13.5	17.7	10.9	14.8	9.4	23.1	9.5	17.1	0.8	4.7	4.5	9.3
Ta	1.6	1.2	1.3	1.5	1.0	1.3	0.8	2.1	0.8	1.4	0.1	0.3	0.3	1.1
Zr	62.4	45.7	32.9	31.6	38.6	59.1	34.8	21.6	31.7	27.2	6.6	41.1	21.9	58.4
Hf	1.8	1.8	1.4	1.4	1.5	1.8	1.3	1.1	1.3	1.2	0.1	1.1	0.7	1.6
Sn	6.4	6.7	3.5	3.1	3.4	4.1	1.1	1.9	2.2	3.6	0.1	0.6	0.4	0.1
Pb	22.2	22.8	12.4	11.2	13.3	17.4	9.2	4.9	8.9	14.6	0.6	2.3	2.8	3.0
U	0.45	0.19	0.21	0.43	0.49	0.49	0.74	0.20	0.18	0.25	0.09	0.14	0.12	2.20
Th	1.57	0.55	0.70	0.85	0.59	1.23	1.87	0.62	0.48	0.77	0.14	0.45	0.33	1.55
La	33.4	36.0	30.4	34.3	30.2	34.3	17.2	15.4	19.6	38.8	1.52	6.12	8.81	10.6
Ce	87.4	95.8	77.6	88.6	79.7	85.5	41.6	38.7	50.4	99.9	2.62	15.6	22.3	25.4
Pr	12.9	14.5	11.5	13.1	12.0	12.4	6.0	5.6	7.5	14.4	0.31	2.32	3.23	3.44
Nd	66.7	75.3	58.6	67.6	61.9	60.9	29.7	28.1	37.6	73.1	0.92	11.1	15.2	15.6
Sm	15.2	17.4	13.2	15.2	13.8	13.6	6.71	6.32	8.63	16.5	0.22	2.63	3.23	3.42
Eu	6.24	6.96	5.84	6.17	6.25	6.00	3.51	2.88	4.22	6.74	0.05	4.62	6.14	5.65
Gd	13.3	15.0	11.3	13.3	11.8	11.8	5.97	5.28	7.77	14.2	0.11	2.03	2.70	2.75
Tb	1.53	1.73	1.32	1.57	1.41	1.35	0.73	0.64	0.90	1.65	0.02	0.27	0.32	0.36
Dy	6.76	7.64	5.84	6.95	6.15	5.99	3.32	2.94	4.20	7.28	0.10	1.20	1.46	1.70
Ho	1.10	1.22	0.99	1.17	1.04	0.95	0.57	0.47	0.72	1.22	0.02	0.21	0.23	0.30
Er	2.25	2.43	1.89	2.29	2.01	1.94	1.18	1.02	1.43	2.38	0.05	0.44	0.53	0.71
Tm	0.26	0.27	0.22	0.24	0.22	0.23	0.14	0.12	0.17	0.27	0.01	0.06	0.07	0.10
Yb	1.35	1.43	1.12	1.37	1.11	1.18	0.77	0.65	0.91	1.41	0.03	0.34	0.43	0.53
Lu	0.19	0.19	0.16	0.19	0.16	0.16	0.11	0.10	0.13	0.20	0.00	0.06	0.07	0.09

Table 11. Concentrations of trace elements (ppm) in rocks from the granitoid and foidolite series

Element	Syenogranite			Quartz syenite				Pulaskite		Ijolite		Aegirin-ite	Nepheline syenite		Laur-dalite
	GV-117	2703/3	GV-113	GV-102	GV-103	GV-110	GV-118	GV-104	GV-109	GV-1/9-A	GV-100	GV-114	GV-107	GV-1/2	GV-111
Li	14.1	4.80	15.8	9.42	32.0	12.7	10.2	15.4	20.4	2.05	34.1	6.52	3.31	4.03	4.10
Rb	87.3	141	102	63.8	76.2	92.3	59.1	105	116	48.9	61.0	3.55	76.4	111	105
Cs	0.93	1.53	1.20	0.66	0.67	0.49	0.71	0.62	1.29	0.07	2.69	0.04	0.20	0.31	0.95
Sr	27.4	16.9	64.8	20.8	197	163	246	369	221	814	1152	961	931	885	1240
Ba	134	64.9	969	181	637	434	815	578	223	282	325	220	577	2059	1586
Sc	0.2	0.0	3.2	0.4	1.8	2.1	1.6	1.5	1.9	12.0	5.2	3.0	2.1	2.4	3.6
V	2.9	1.4	2.9	0.4	3.4	1.2	1.8	1.4	1.2	86.7	11.1	32.6	9.5	23.2	16.6
Cr	91.1	10.3	36.0	32.2	27.6	23.2	24.2	12.3	3.2	58.8	26.8	67.8	14.8	23.1	37.2
Co	2.0	0.0	1.4	0.6	1.8	1.9	1.4	3.6	4.0	16.4	4.5	8.5	3.2	7.4	4.6
Ni	13.5	0.8	7.4	7.4	7.9	5.5	6.7	2.7	4.8	29.9	7.1	39.6	13.1	10.0	8.0
Cu	23.8	2.6	10.0	9.2	12.3	8.9	12.3	8.7	10.1	9.4	8.8	10.3	16.7	13.1	10.7
Zn	158	0.0	73.1	41.7	130	87.7	83.4	56.8	69.7	83.4	87.7	139	47.2	107	120
Y	50.6	28.4	17.0	9.3	13.0	19.0	13.6	7.8	9.7	14.2	13.2	30.5	13.9	5.0	8.3
Nb	124	92.9	39.9	15.2	25.8	54.9	22.4	47.4	95.3	25.3	86.8	5040	15.8	32.3	367
Ta	10.2	7.1	3.1	1.1	1.6	2.6	1.0	1.7	3.4	1.2	3.7	83.2	1.2	2.7	15.3
Zr	824	234	90.6	177	240	322	153	33.8	81.2	896	1569	3127	24.0	106	542
Hf	22.9	12.1	3.2	5.0	6.5	7.7	4.0	1.4	2.8	23.8	40.2	90.6	0.5	3.5	15.4
Sn	1.4	0.0	2.3	1.2	1.9	0.9	1.4	0.0	0.4	2.9	15.2	89.1	0.1	0.3	8.7
Pb	438	9.2	8.4	2.6	4.0	3.6	8.3	5.8	4.3	2.6	3.4	307	1.5	2.3	7.0
U	712	2.18	1.12	0.56	0.96	0.88	0.67	1.74	1.19	0.17	1.78	682	0.27	0.34	12.3
Th	12.4	17.3	5.59	1.73	2.38	3.76	1.68	1.99	1.70	0.72	3.47	188	0.53	0.90	2.66
La	68.2	39.6	5.2	7.4	20.7	31.1	27.5	28.0	33.5	25.1	13.1	119	45.7	13.3	15.0
Ce	148	107	27.2	18.0	63.6	81.2	62.1	61.9	76.9	71.5	32.6	337	115	29.8	38.3
Pr	17.7	11.1	2.41	2.41	6.62	9.93	8.72	7.42	9.61	10.3	4.64	40.6	15.9	3.94	4.83
Nd	74.0	44.2	11.1	10.9	27.4	41.1	35.6	27.6	36.1	45.1	19.4	152	66.6	15.8	19.1
Sm	16.3	8.72	3.62	2.61	5.51	8.62	7.22	4.83	6.53	9.64	4.84	27.9	12.7	3.13	3.72
Eu	2.96	1.33	1.28	0.72	1.59	2.29	2.25	1.38	1.41	3.04	1.65	8.91	3.77	1.14	1.34
Gd	14.21	7.56	3.50	2.43	4.17	6.53	5.34	3.40	4.56	7.58	4.07	16.5	9.18	2.43	2.88
Tb	1.99	1.22	0.60	0.37	0.56	0.89	0.72	0.42	0.54	0.94	0.56	2.10	1.08	0.31	0.41
Dy	10.74	7.07	3.71	2.00	2.93	4.50	3.40	1.99	2.62	4.00	2.99	9.84	4.48	1.35	1.98
Ho	2.07	1.38	0.72	0.39	0.56	0.80	0.60	0.34	0.44	0.61	0.58	1.50	0.66	0.22	0.37
Er	4.70	3.50	1.85	0.92	1.37	1.91	1.42	0.75	0.92	1.46	1.84	3.47	1.20	0.52	0.85
Tm	0.63	0.48	0.29	0.13	0.21	0.25	0.19	0.09	0.12	0.24	0.41	0.49	0.14	0.07	0.14
Yb	3.30	3.00	1.77	0.76	1.24	1.62	1.20	0.53	0.76	1.88	3.63	3.97	0.63	0.49	0.90
Lu	0.46	0.43	0.27	0.13	0.20	0.26	0.17	0.08	0.11	0.38	0.81	0.84	0.08	0.08	0.16

Table 12. Sm–Nd isotopic data on rocks from the Gremyakha–Vyrmes Massif

Rock	Sample	Sm, ppm	Nd, ppm	$^{147}Sm/^{144}Nd$	$^{143}Nd/^{144}Nd$	$(^{143}Nd/^{144}Nd)_{(T)}$	ε_{Nd}	T(DM)*	T(DM)**
Peridotite	GV-50	58.61	13.06	0.1348	0.511797	0.510129	–1.5	2.601	2.485
Gabbro	GV-51	37.60	8.59	0.1382	0.511837	0.510127	–1.5	2.638	2.488
Gabbro	GV-43	29.72	6.77	0.1377	0.511862	0.510158	–0.9	2.571	2.438
Magnetite gabbro	GV-44	0.94	0.21	0.1361	0.511788	0.510104	–2.0	2.662	2.525
Monzosyenite	GV-106	15.30	3.34	0.1319	0.511783	0.510151	–1.0	2.535	2.450
Pulaskite	GV-104	17.15	3.05	0.1075	0.511558	0.510228	0.5	2.276	2.326
Pulaskite	GV-109	36.11	6.49	0.1086	0.511483	0.510139	–1.3	2.407	2.469
Syenogranite	GV-113	7.60	2.32	0.1844	0.51233	0.510049	–3.1	4.230	2.614
Quartz syenite	GV-110	41.09	8.60	0.1265	0.511709	0.510144	–1.2	2.507	2.461
Quartz syenite	GV-118	35.65	7.04	0.1194	0.511635	0.510158	–0.9	2.438	2.439
Quartz syenite	GV-103	27.42	5.51	0.1215	0.511430	0.509927	–5.4	2.828	2.809
Ijolite	GV-100	15.68	4.01	0.1547	0.512045	0.510131	–1.4	2.839	2.482
Ijolite	GV-1/9A	45.89	9.62	0.1268	0.511841	0.510272	1.3	2.287	2.255
Laurdalite	GV-111	19.08	3.70	0.1173	0.511712	0.510261	1.1	2.364	2.273
Nepheline syenite	GV-1/2	10.83	2.21	0.1235	0.511745	0.510217	0.2	2.265	2.344

Note: * The depleted mantle parameters for model age T(DM) calculations were compiled from (DePaolo et al., 1991).
** Model ages T(DM) were calculated following the procedure in (Liew and Hofmann, 1998): $(^{143}Nd/^{144}Nd)_{DM} = 0.513149$, $(^{147}Sm/^{144}Nd)_{DM} = 0.2136$, $(^{147}Sm/^{144}Nd)_{CC} = 0.12$.

sedimentary unit (Table 13). The comparison of the Pechenga volcanics and the Gremyakha–Vyrmes gabbroids indicates that they are characterized by elevated concentrations of Fe and Ti and similar distributions of trace elements. According to (Hanski and Smolkin, 1995), the geochemical and isotopic characteristics of the picrites suggest that they were contributed by a depleted mantle source (DM). With regard for the results of geodynamic reconstructions, the Pechenga ferropicrites could be emplaced during the maximum opening the Proterozoic rift structure, which facilitated the inflow of the ultrabasic melts with mantle isotopic signatures. In ε_{Nd}–T and $^{87}Sr/^{86}Sr$–T diagrams (Fig. 13), the Pechenga ferropicrites have the highest ε_{Nd} values and the lowest $^{87}Sr/^{86}Sr$ ratios, which suggests the minimum involvement of crustal material. At the same time, the data points of rocks from the Gremyakha–Vyrmes Massif bridge the compositional gap between the rocks of the late rifting stage and the final magmatic phases (Litsa–Ara Guba granodiorites). The model ages calculated for the Gremyakha–Vyrmes Massif coincide with those of the Pechenga picritic volcanics and are close to 2450 Ma, i.e., to the age of the onset of the development of the whole Pechenga–Varzuga rift structure. It is reasonable to suggest that the values obtained for $T_{Nd}(DM)$ correspond to the time of the separation of the ferropicritic melts from the mantle source before the rifting evolutionary stage of this structure. The further evolution of the ferropicritic melts, which were parental for the ultrabasic and granitoid series of the Gremyakha–Vyrmes Massif, proceeded within the crust.

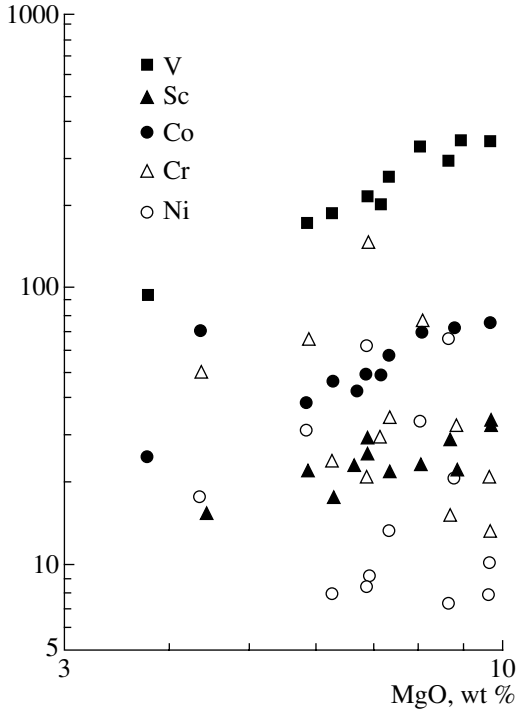

Fig. 8. Correlation between the concentrations of trace elements and MgO in rocks of the ultrabasic series.

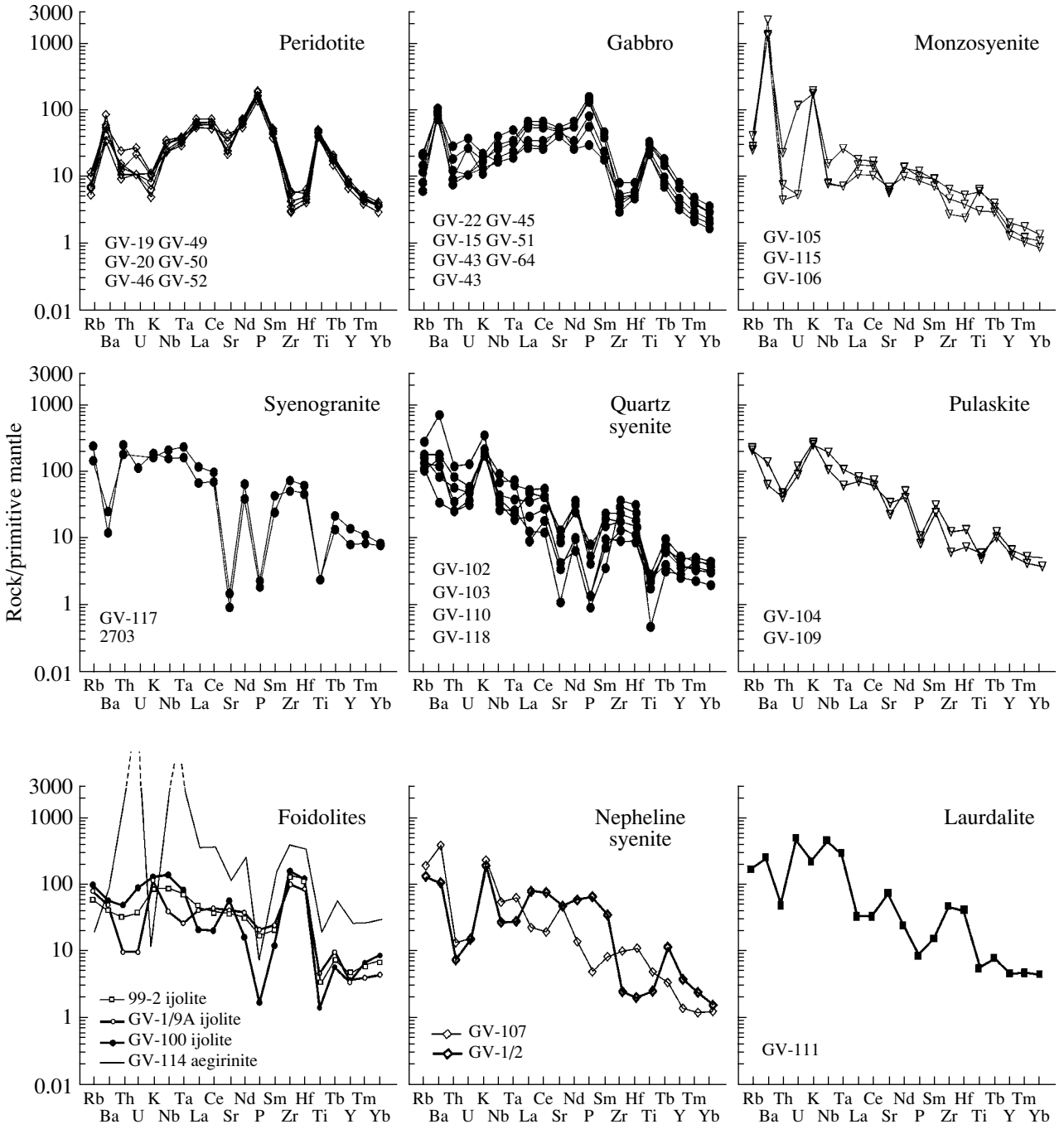

Fig. 9. Concentrations of trace elements normalized to the primitive mantle (McDonough et al., 1991) in rocks of the Gremyakha–Vyrmes Massif.

Granitoid series. The geochemical characteristics of this series testify that the granitoids affiliate with A-type subalkaline and alkaline varieties (Eby, 1990; Barbarin, 1999). It is logical to consider two alternative hypotheses concerning the genesis of the granitoids: (i) these granitoids are not genetically related to the other rocks of the massif, and (ii) the granitoids are differentiates of a melt that was also parental for the ultrabasic rocks of the massif (Polkanov et al., 1967). The former hypothesis was put forth by Kukharenko et al. (1971). This hypothesis denied the affiliation of the granitoids with the Gremyakha–Vyrmes Massif and suggested the existence of an independent granite intrusion. Nevertheless, the similarities between the isotopic dates and the occurrence of hybrid rock varieties, whose compositions are intermediate between those of

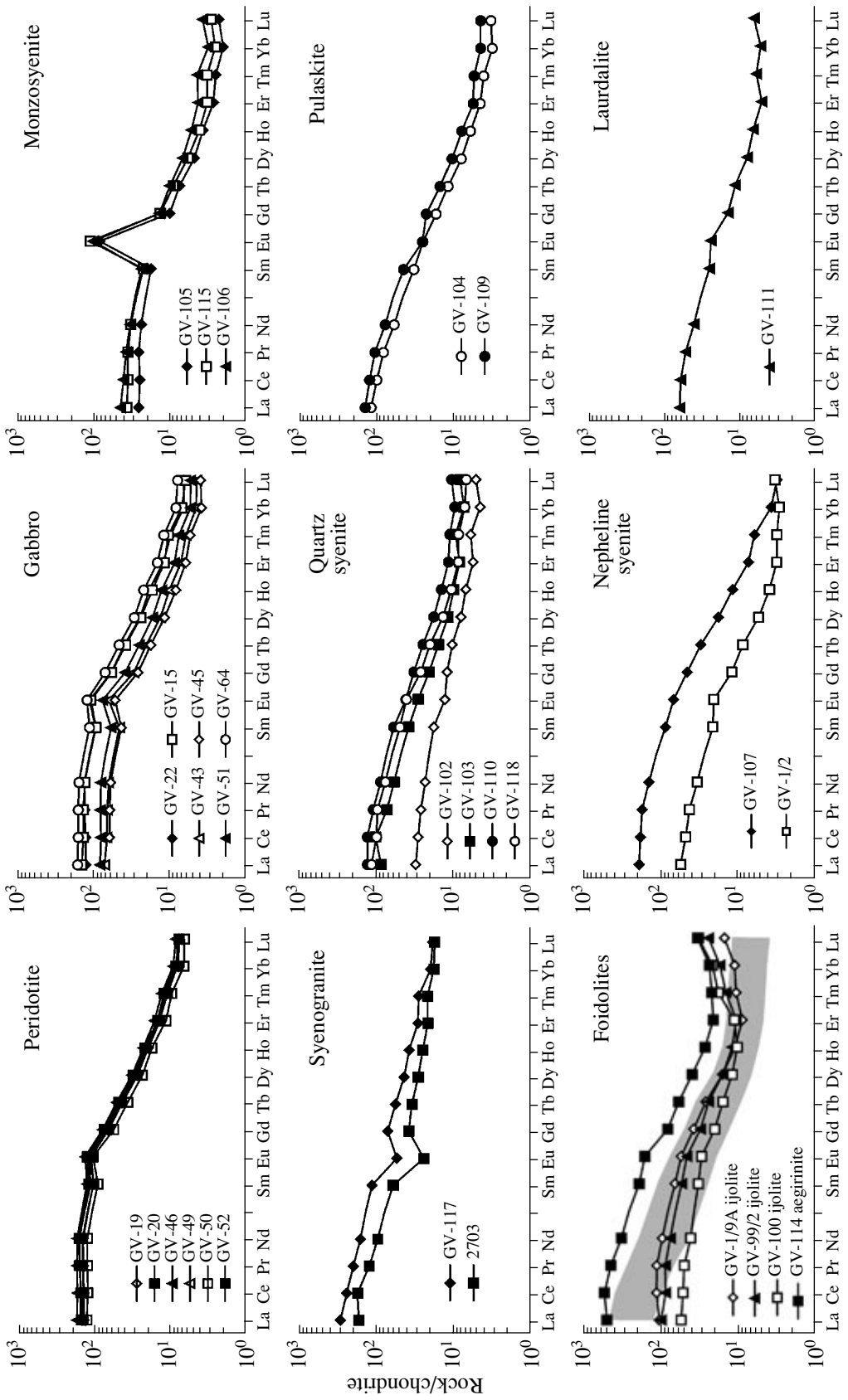

Fig. 10. Chondrite-normalized (Anders and Grevesse, 1989) REE patterns for rocks of the Gremyakha–Vyrmes Massif.
The diagram for the foidolites demonstrates the REE fractionation in the Paleozoic ijolites of alkaline–ultrabasic massifs in the province according to (Arzamastsev et al., 2002).

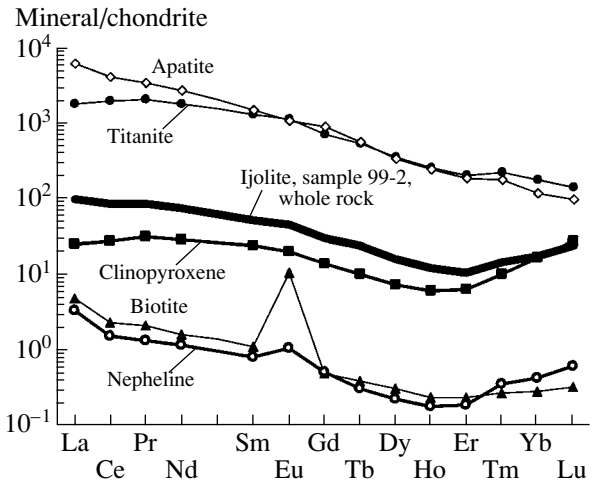

Fig. 11. Chondrite-normalized (Anders and Grevesse, 1989) REE patterns for ijolite (sample 99-2) and its minerals.

the granitoids and foidolites and between granitoids and ultrabasites, makes it impossible to regard these rocks as an autonomous intrusion. The only geological body in the northeastern Baltic Shield that can be compared with the granitoids of the Gremyakha–Vyrmes Massif is the nearby Litsa–Ara Guba Complex. However, the rocks of this composition are younger (1765 ± 7 Ma; Bayanova, 2004), and their isotopic characteristics suggest the significant involvement of crustal material (Fig. 12): ε_{Sr} from 47.3 to 165.1 and ε_{Nd} from –6.3 to –7.8 (Pushkarev, 1990; Timmerman and Daly, 1995). Moreover, the Litsa–Ara Guba Complex belongs to the granodiorite–granite series, whose rocks display no alkaline differentiation trend (Batieva and Vinogradov, 1991). Hence, the rocks of the granitoid series of the Gremyakha–Vyrmes Massif have no analogues among the Proterozoic granitoids of northeastern Fennoscandia, and, at the same time, the geochemical characteristics of these granitoids point to their complementary character with the ultrabasic rocks of the massif (the negative Ba, P, and Ti anomalies of the syenogranites and their positive K, Zr, and Hf anomalies are complementary with the anomalies of opposite sign displayed by the gabbro and peridotites). This allowed us to consider the model for the genesis of the granitoids as a result of the evolution of the magmas that were parental for the ultrabasic series of the Gremyakha–Vyrmes Massif.

Foidolite series. The finds of carbonate veins with mantle signatures within the massif (Savatenkov et al., 1999) suggest that this massif contains the whole alkaline–ultrabasic series of melteigites, ijolites, nepheline syenites, and carbonatites. The isotopic–geochemical characteristics of the foidolites are notably different from those of the all other rocks of the massif. Together

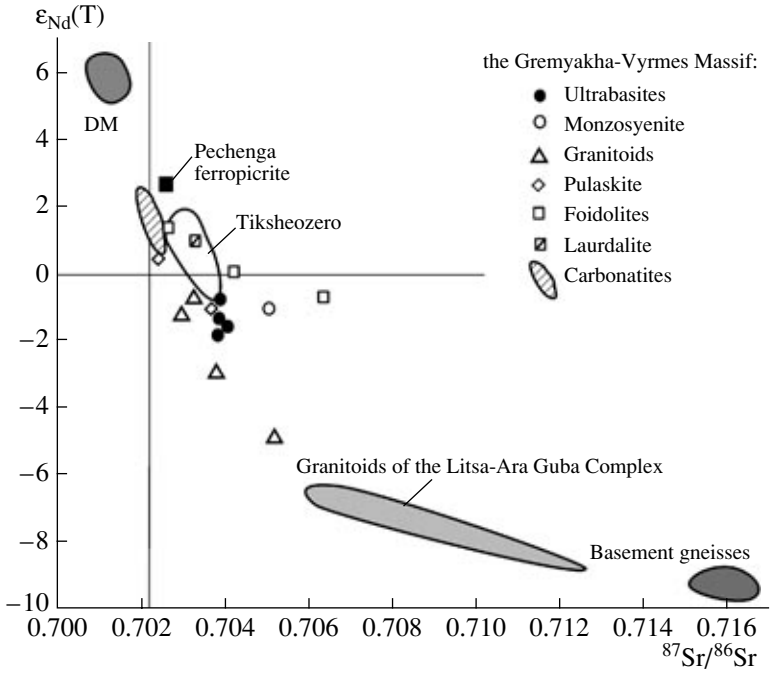

Fig. 12. $^{87}Sr/^{86}Sr$ vs. $\varepsilon_{Nd}(T)$ diagram for Proterozoic rocks of the Kola Peninsula. Based on data on the Tiksheozero Massif (Belyatskii et al., 2000), carbonatites of the Gremyakha–Vyrmes Massif (Savatenkov et al., 1999), Pechenga ferropicrites (Hanski and Daly, 1995), granitoids of the Litsa–Ara Guba Complex (Pushkarev, 1990; Timmerman and Daly, 1995), and basement rocks (Savatenkov et al., 1998; Timmerman and Daly, 1995). The characteristics of the depleted mantle (DM) are given after (DePaolo et al., 1991). All data are recalculated for an age of 1885 Ma.

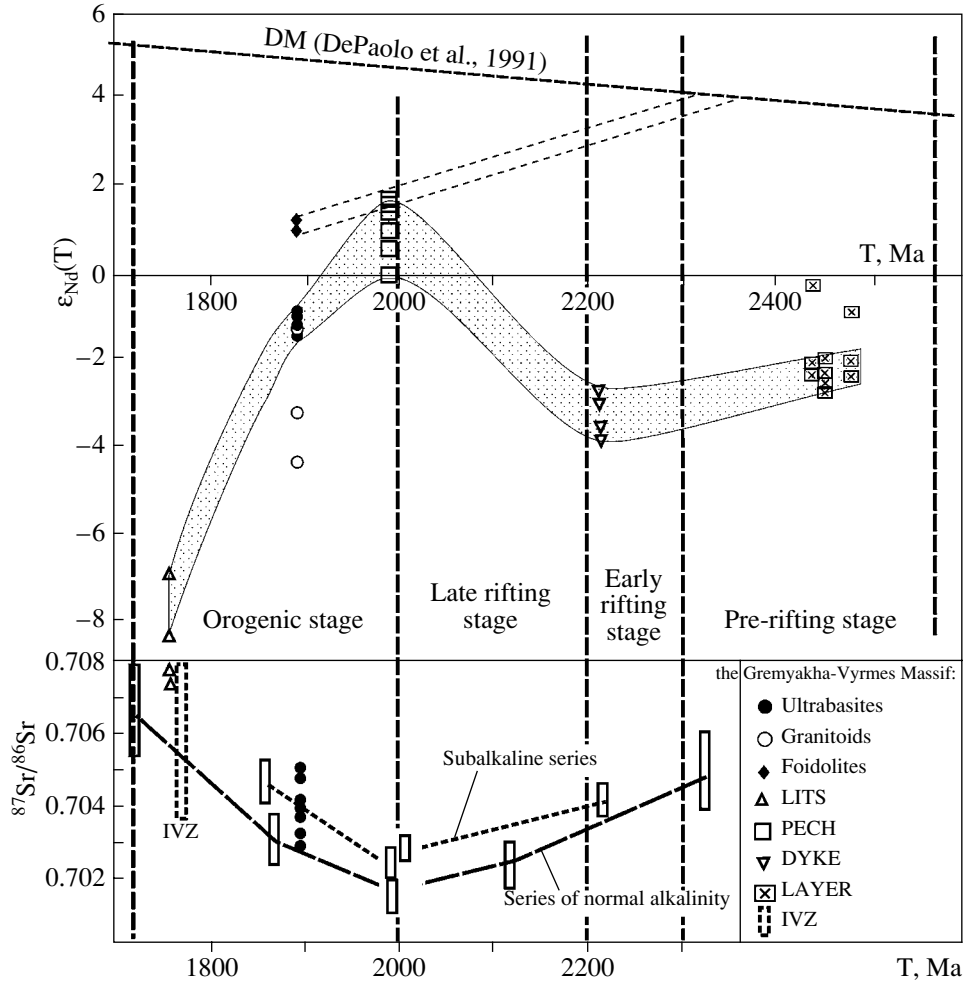

Fig. 13. Diagram showing variations in the $\varepsilon_{Nd}(T)$ and $^{87}Sr/^{86}Sr$ of Proterozoic magmatic rocks in northeastern Fennoscandia with time.

The diagram is modified after (Balashov, 1996; Smolkin, 1997) with the use of data from (Timmerman and Daly, 1995; Fedotov and Amelin, 1998; Bayanova, 2004). LITS—granitoids of the Litsa–Ara Guba Complex, PECH—volcanic ferropicrites and gabbro–wehrlites of the Pechenga structure, LAYER—layered basic intrusions, DYKE—dolerites of the dike swarm in the northern surroundings of the Pechenga structure. IVZ—volcanics of the Imandra–Varzuga zone. Rifting stages are given after (Smolkin, 1997). Thin dashed lines show the model ages of foidolites from the Gremyakha–Vyrmes Massif.

with the carbonatites, they define a trend suggesting the predominance of another, more depleted source (Fig. 12). The similarities between the Sr–Nd isotopic characteristics of the Gremyakha–Vyrmes foidolites and the rocks of the Tiksheozero Massif suggest that the parental alkaline–ultrabasic melts of these rocks were derived from an autonomous mantle source and were the least contaminated by crustal material.

Models for Melt Evolution

Proceeding from the idea that the Gremyakha–Vyrmes Massif was produced by two independent parental mantle melts (ferropicritic and alkaline-ultrabasic), we consider the following models for their evolution and interaction. Material balance calculations for major oxides and all REE were carried out by the formulas conventionally utilized to describe fractional crystallization coupled with contamination. In addition, to test the results, we used the PELE computer program (Boudreau, 1999), which is a MS Windows-adapted variant of the MELTS program package for thermodynamic simulations (Ghiorso et al., 1994). The input parameters for the simulations (the compositions of the parental melts, contaminant, and fractionated phases and the distribution coefficients) are summarized in Table 14 and are also given in Tables 2, 4, and 8–11.

The first stage of the simulations involved the calculation of a fractionation model for the parental ferropicritic melt, which was assumed to correspond to the Pechenga volcanic rocks (sample 2728/773) and produced a magma of composition corresponding to the

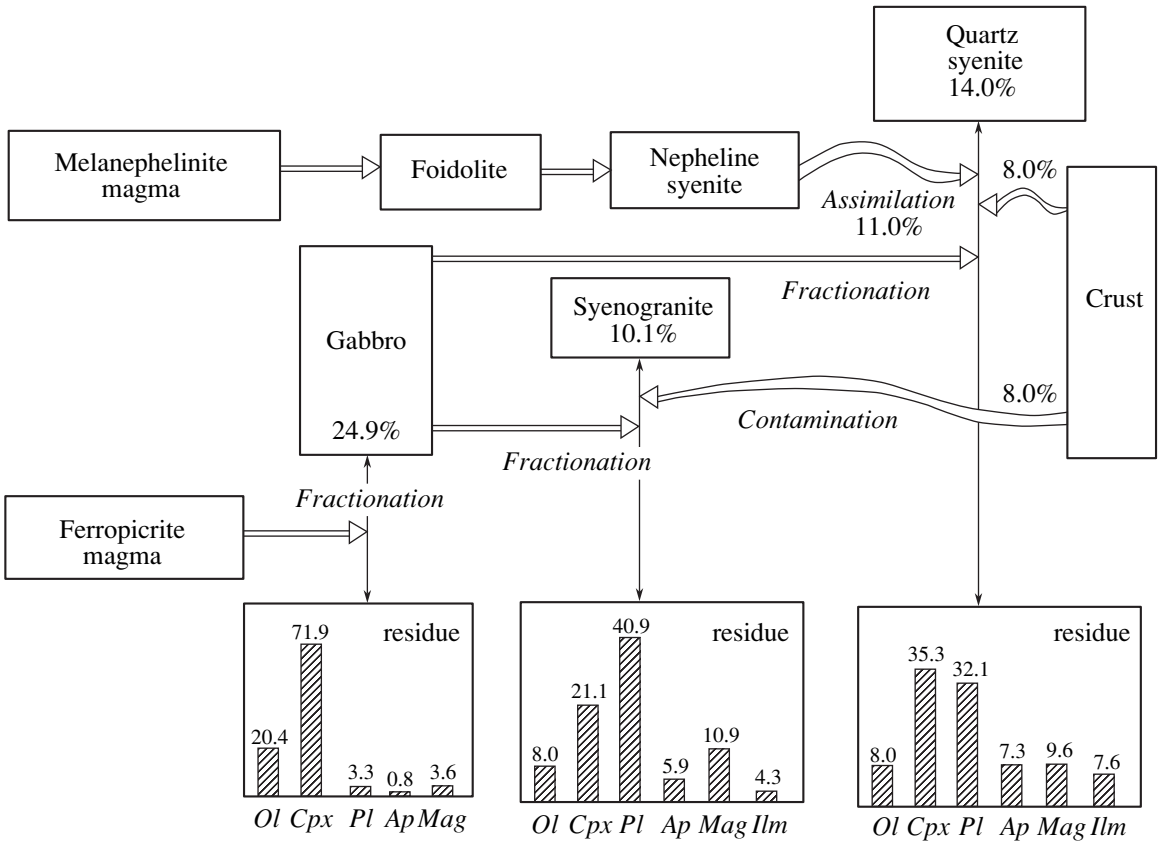

Fig. 14. Evolution of the parental melts of the Gremyakha–Vyrmes Massif (see text for explanations).

average composition of the ultrabasic series of the Gremyakha–Vyrmes Massif (sample GV-43). The data presented in Table 15 and Fig. 14 indicate that 24.9% of the gabbroid melt can be obtained by the fractionation of 20.4% olivine, 71.9% clinopyroxene, and minor amounts of plagioclase, apatite, and titanomagnetite. The composition of the residue generally corresponds to the composition of the naturally occurring cumulates of the ultrabasic series of this massif. We calculated the fractionation of REE with regard for the proportions of these phases and demonstrated that a satisfactory consistency between the simulated REE concentrations and those measured in sample GV-43 can be obtained by 30–35% fractionation of the ferropicritic melt, which is in general agreement with the major-element estimates (Fig. 15a).

During the second stage of our simulations, we tested the model for the genesis of the granitoid melts during the evolution of the basic magma. The assumed parental melt had a composition close to the average composition of the ultrabasic series of the massif (sample GV-43), and the derivatives of this melt were taken up to be the syenogranite (sample GV-117) and quartz syenite (sample GV-110). Our simulations indicate that satisfactory results with both products of the granitoid magmas can be yielded only by 8–10% crustal contamination of the parental melts (Fig. 15b, Table 15). Furthermore, a significant role in the origin of the alkaline phase of the granitoids (quartz syenites) was played by the mixing of the basaltic magma with small portions a phonolite melt of composition close to that of the nepheline syenite of the massif (Fig. 15c). Given the presence of monzosyenites (along with gabbroids of normal alkalinity) in the ultrabasic series of the Gremyakha–Vyrmes Massif, it is logical to believe that the mixing of the ferropicritic and alkaline melts occurred under crustal conditions, early during the origin of the massif.

The calculation of the evolutionary model for the melanephelinitic magmas revealed the possibility of obtaining a typical succession of the derivatives of the alkaline–ultrabasic series, from olivine and pyroxene cumulates to melteigites, ijolites, and nepheline syenites. A similar but more complete trend is characteristic of Paleozoic alkaline–ultrabasic massifs of the province (such as Kovdor, Vuorijarvi, and Salmagora). Compared to their Paleozoic analogues, the rocks of the massif are richer in SiO_2 and poorer in CaO and alkalis, because of which the massif contains no melilite-bearing rocks.

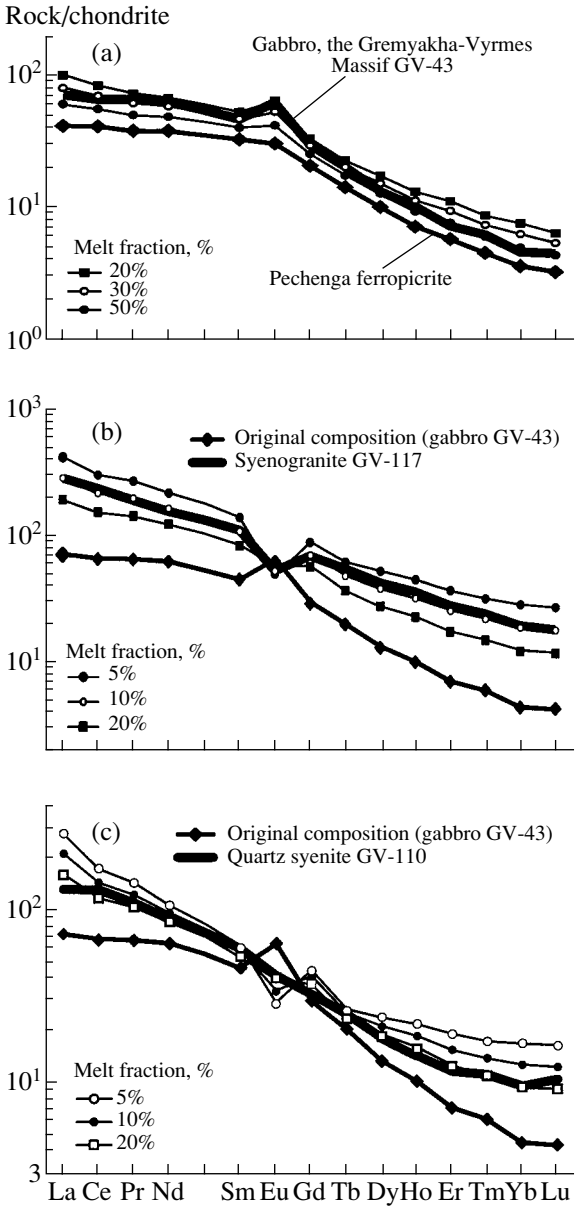

Fig. 15. Chondrite-normalized REE patterns of the parental melts and their fractional crystallization products for (a) ferropicrite from the Pechenga volcanics and gabbro of the Gremyakha–Vyrmes Massif, (b) original gabbro and syenogranite at the assimilation of 8% crustal material, and (c) original gabbro and quartz syenite at the assimilation of 8% crustal material and the addition of 11% phonolite melt. The diagram demonstrates the calculated REE concentrations during the crystallization of the parental melt.

Role of Alkaline Melts in the Evolution of Magmatism in the Northeastern Baltic Shield

Along with ijolite–carbonatite and nepheline syenite series of the Tiksheozero Massif in northern Karelia and the Almunge Massif in Sweden, the foidolites of the Gremyakha–Vyrmes Massif are the oldest products of alkaline and carbonatite magmatism in the Baltic Shield. The appearance of alkaline melts in the northern

Table 13. Concentrations of major (wt %) and trace (ppm) elements in ferropicrites from the Pechenga zone

Oxide	3077/313	3077/350	2728/773
SiO_2	44.07	40.89	39.50
TiO_2	2.02	2.10	2.30
Al_2O_3	6.40	7.60	5.79
Fe_2O_3	3.39	3.65	4.91
FeO	9.73	10.16	10.42
MnO	0.17	0.17	0.19
MgO	12.10	12.77	12.55
CaO	11.26	11.28	12.82
Na_2O	0.08	0.13	0.12
K_2O	0.04	0.04	0.13
P_2O_5	0.18	0.20	0.27
CO_2	4.28	4.09	4.43
H_2O^+	5.94	6.91	6.25
H_2O^-	0.12	0.04	0.07
Total	99.78	100.03	99.75
Li	7.95	10.3	13.5
Rb	1.77	9.60	15.2
Sr	157	96.3	193
Ba	8.11	138	46.6
Sc	25.7	32.1	25.5
V	229	274	249
Cr	1215	924	1023
Co	98.9	60.9	82.9
Ni	1225	525	841
Cu	324	179	138
Zn	210	88.6	109
Ga	7.39	9.81	7.49
Y	16.9	21.4	15.6
Nb	14.2	18.2	17.3
Ta	0.93	1.15	1.14
La	43.6	14.5	8.34
Ce	76.0	36.7	23.0
Pr	8.10	5.21	3.56
Nd	29.4	22.2	17.6
Sm	5.87	5.73	5.18
Eu	1.71	1.98	1.57
Gd	5.28	5.63	4.38
Tb	0.72	0.87	0.67
Dy	3.66	4.64	3.53
Ho	0.71	0.89	0.66
Er	1.73	2.18	1.56
Tm	0.25	0.31	0.22
Yb	1.40	1.77	1.23
Lu	0.21	0.25	0.18
Pb	26.5	1.36	1.64

Note: Ferropicrites from the upper (samples 3077/313 and 3077/350) and lower (sample 2728/773.2) parts of the stratigraphic succession of lavas from the Matertskaya Subformation IV of the volcanic sequence.

Table 14. Rock compositions (ppm) and the mineral/melt distribution coefficients (D) used in the model simulations of fractional crystallization and assimilation

Element	Ferropicrite	Archean gneiss	D_{Ol}	D_{Cpx}	D_{Pl}	D_{Pl}	D_{Ap}	D_{Mag}	D_{Ilm}
La	8.34	33.0	0.00001	0.049	0.1477	0.3	5.16	0.2	0.006
Ce	23.0	61.0	0.00002	0.07	0.0815	0.24	6.34	0.2	0.006
Pr	3.56	–	0.00005	0.12*	0.048*	0.2*	6.45	0.2*	0.007*
Nd	17.6	16.8	0.0001*	0.178	0.0551	0.17	6.6	0.2	0.008
Sm	5.18	2.20	0.0005	0.293	0.0394	0.13	6.3	0.2	0.010
Eu	1.57	0.91	0.001*	0.31*	1.125	2.11	3.77	0.06	0.013*
Gd	4.38	2.10	0.002*	0.34*	0.031	0.09	6	0.12*	0.015
Tb	0.67	0.27	0.003	0.36*	0.038*	0.088*	5.79	0.2	0.017*
Dy	3.53	–	0.01*	0.38	0.0228	0.086	5	0.2*	0.02
Ho	0.66	–	0.01	0.387*	0.035*	0.085*	4.5	0.2*	0.025*
Er	1.56	0.66	0.018*	0.391*	0.0202	0.084	4	0.2	0.03
Tm	0.22	–	0.027*	0.395*	0.033*	0.08*	3.9	0.2	0.04*
Yb	1.23	0.43	0.037	0.4	0.0232	0.077	3.24	0.2	0.05
Lu	0.18	0.062	0.05	0.449	0.0187	0.062	3.4	0.645	0.06
Reference	–	[1]	[2]	[3]	[4]	[5]	[5]	[6]	[4]

Note: The assumed parental ferropicrite melt corresponded in composition to ferropicrite (sample 2728/773) of the Matertskaya Subformation IV of the volcanic sequence, Pechenga structure. The assumed assimilated crustal material corresponded in composition to Archean plagioclase gneiss from the lower part of the Kola Superdeep Borehole. References: [1] Vetrin et al., 1999; [2] Beattie, 1994; [3] Johnson, 1998; [4] Fujimaki and Tatsumoto, 1984; [5] Caroff et al., 1993; [6] Nash and Crecraft, 1985.
* The distribution coefficient was calculated by interpolating the values for the neighboring REE.

(Gremyakha–Vyrmes Massif) and central (Soustova Massif) parts of the Pechenga–Varzuga rift zone was directly related to the final evolutionary stage of this largest structure in the Proterozoic. The weak magmatic activity during the following more than 1-Ga time span testifies to the stability of the subcratonic region of the mantle keel during plate tectonic processes. During this long-lasting amagmatic period, the only indications of the existence of the anomalously enriched mantle were volumetrically insignificant products of mantle magmatism: lamproites of the Kuhmo–Kostomuksha area in northern Karelia with an age of 1230 Ma (I_{Sr} = 0.70382, ε_{Nd} = –9.1; Belyatskii et al., 1997) and kimberlites in the Kaavi–Kuopio area in central Finland with an age of ~600 Ma (O'Brien et al., 2004). Thus, the plume–lithospheric interaction that started at 1.88 Ga produced domains in the mantle keel of the Baltic Shield that were enriched in incompatible elements and were able to generate alkaline and carbonatite melts. It is reasonable to believe that the sublitospheric domains of mantle material metasomatized in the Proterozoic were later (in Paleozoic time) reactivated in the course of magmatic activity that occurred in the northeastern part of Fennoscandia and gave rise to the largest of Khibina and Lovozero, alkaline intrusions and carbonatite massifs.

CONCLUSIONS

1. The Proterozoic Gremyakha–Vyrmes Massif consists of three autonomous intrusive series, which were produced within a relatively brief period of time (1885 ± 20 Ma) in the following succession: (i) ultrabasic layered series, (ii) granitoid series, and (iii) foidolite series. The occurrence of subalkaline ultrabasites in the massif, along with rocks of composition intermediate between the gabbroids and syenogranites and between the gabbroids and foidolites, provides evidence not only of the contact effect of the younger magma injections but also of the mixing of the alkaline and ultrabasic melts.

Table 15. Composition (wt %) of the parental melts (*Par*) and their products (*Pro*) and the parameters of the model simulations of the fractional crystallization of rocks from the Gremyakha–Vyrmes Massif

Component	Stage 1				Stage 2a				Stage 2b			
	Par.	Pro.			Par.	Pro.			Par.	Pro.		
	Fe-picrite	Gabbro GV-43	Obser. – calc.	Residue	Gabbro GV-43	Syenogranite GV-117	Obser. – calc.	Residue	Gabbro GV-43	Quartz syenite GV-110	Obser. – calc.	Residue
SiO_2	45.89	46.21	–0.06	45.89	46.21	76.77	–0.35	43.40	46.21	63.73	–0.23	39.92
TiO_2	1.50	3.61	0.03	0.76	3.61	0.40	0.04	3.94	3.61	0.48	0.16	5.29
Al_2O_3	5.30	13.66	0.09	2.44	13.66	10.24	0.55	13.49	13.66	16.21	0.95	10.26
FeO	16.95	14.26	–0.01	17.86	14.26	4.66	–0.06	15.46	14.26	6.05	0.10	18.18
MnO	0.25	0.20	–0.07	0.36	0.20	0.08	0.03	0.18	0.20	0.13	0.01	0.24
MgO	14.45	5.95	0.06	17.21	5.95	0.13	0.39	6.19	5.95	0.13	0.52	5.27
CaO	13.71	10.60	0.11	14.63	10.60	0.31	0.64	11.08	10.60	1.16	0.79	14.91
Na_2O	1.38	3.80	0.05	0.52	3.80	3.60	0.18	3.63	3.80	7.02	–0.54	2.58
K_2O	0.15	0.50	0.02	0.01	0.50	3.76	–0.10	0.25	0.50	4.97	–0.95	0.1
P_2O_5	0.42	1.22	–0.13	0.32	1.22	0.05	–0.93	2.39	1.22	0.12	–0.81	3.24
Σr^2			0.05				1.90				3.75	
Proportion of derivatives, %		24.9		75.1		10.1		81.9		14.0		67.0
Percentage of contaminant, %					8.0 (gneiss)				19.0 (8% gneiss + 11% phonolite)			
Modal composition of residue (%)												
Ol (111/275)				20.4				8.0				8.0
Cpx (GV-51/23)				71.9				21.1				35.3
Pl (GV-51/23)				3.3				40.9				32.1
Ap				0.8				5.9				7.3
Mag				3.6				10.9				9.6
Ilm								4.3				7.6

Note: *Ol*—olivine, *Cpx*—clinopyroxene, *Pl*—plagioclase, *Ap*—apatite, *Mag*—magnetite, *Ilm*—ilmenite. **Obser. – calc.** means the difference between oxide concentrations for the original and calculated model compositions. Numerals in parentheses correspond to the numbers of chemical analyses in Tables 2–5.

2. The most probable parental magmas of the ultrabasic series of the Gremyakha–Vyrmes Massif were ferropicritic melts produced by endogenic activity in the Pechenga–Varzuga rift zone. According to simulation results, the granitoids of the massif were produced by the fractional crystallization of melts genetically related to the gabbro-peridotite melts and the accompanying assimilation of Archean crustal material and mixing with small volumes of alkaline–ultrabasic melts.

3. The occurrence of ultrabasic foidolites and carbonatites in the Gremyakha–Vyrmes Massif indicates that domains of metasomatized mantle material that were enriched in incompatible elements and were able to generate the alkaline and carbonatite melts occurred in the sublithospheric mantle beneath northeastern Fennoscandia as early as 1.88 Ga. The involvement of these domains in plume–lithospheric processes at 0.4–0.36 Ga brought about the formation of peralkaline melts that produced the Paleozoic Kola alkaline province.

ACKNOWLEDGMENTS

Consultations with A.N. Vinogradov (Kola Research Center, Russian Academy of Sciences), who also provided us with rock samples from the Gremyakha–Vyrmes Massif, were useful for the analysis of the geological structure of this massif and the recognition of its major rock groups. The authors thank P.K. Skuf'in (Geological Institute, Kola Research Center, Russian Academy of Sciences) for samples of the Pechenga volcanics and G.L. Vursii (same institute) for excursion to exposures of the layered hyperbasite series of the massif. This study was financially supported by the Russian Foundation for Basic Research (project no. 06-05-64130), program no. 4 of the Earth Science Division, Russian Academy of Sciences, and NATO (Grant EST-CLG-978997).

REFERENCES

1. E. Anders and N. Grevesse, "Abundances of the Elements: Meteoritic and Solar," Geochim. Cosmochim. Acta **53**, 197–214 (1989).
2. A. A. Arzamastsev, F. Bea, L. V. Arzamastseva, and P. Montero, "Rare-Earth Elements in the Rocks and Minerals of Alkaline Intrusions of the Kola Peninsula as Indicators of the Evolution of Alkaline Melts," Ross. Zh. Nauk o Zemle **4** (3), 3–24 (2002).
3. V. V. Balaganskii, V. N. Glaznev, and L. G. Osipenko, "The Early Proterozoic Evolution of the Northeastern Baltic Shield: A Terrane Analysis," Geotektonika, No. 2, 16–28 (1998) [Geotectonics **32** (2), 81 (1998)].
4. Yu. A. Balashov, "Paleoproterozoic Geochronology of the Pechenga-Varzuga Structure, Kola Peninsula," Petrologiya **4** (1), 3–25 (1996) [Petrology **4** (1), 1 (1996)].
5. B. Barbarin, "A review of the Relationships between Granitoid Types, their Origins and their Geodynamic Environments," Lithos **46**, 605–626 (1999).
6. T. B. Bayanova, *Age of the Reference Geological Complexes of the Kola Region and the Duration of Magmatic Processes* (Nauka, St. Petersburg, 2004) [in Russian].
7. F. Bea, A. Arzamastsev, P. Montero, and L. Arzamastseva, "Anomalous Akaline Rocks of Soustov, Kola: Evidence of Mantle-Derived Metasomatic Fluids Affecting Crustal Materials," Contrib. Mineral. Petrol. **140**, 554–566 (2001).
8. P. Beattie, "Systematics and Energetics of Trace-Element Partitioning between Olivine and Silicate Melts: Implications for the Nature of Mineral–Melt Partitioning," Chem. Geol. **117**, 57–71 (1994).
9. B. V. Belyatskii, L. P. Nikitina, E. V. Savva, and L. K. Levskii, "Isotopic Signatures of Lamproite Dikes on the Eastern Baltic Shield," Geokhimiya, No. 6, 658–663 (1997) [Geochem. Int. **35** (6), 575 (1997)].
10. B. V. Belyatskii, M. Tikhomirova, and E. V. Savva, "Age and Genesis of the Proterozoic Alkaline–Ultramafic Tiksheozero Massif, Northern Karelia: Results of Rb–Sr–Nd Isotope Investigations," in *Proceedings of the 1st All-Russia Conference on Isotope Geochronology. Isotope Dating of the Geological Processes: New Methods and Results. Moscow, Russia, 2000* (GEOS, Moscow, 2000), pp. 63–65 [in Russian].
11. A. Berthelsen and M. Marker, "Tectonics of the Kola Collision Suture and Adjacent Archaean and Early Proterozoic Terrains in the Northeastern Region of the Baltic Shield," Tectonophysics **126**, 31–55 (1986).
12. A. E. Boudreau, "PELE: a Version of the MELTS Software Program for the PC Platform," Comp. Geosci. **25**, 21–203 (1999).
13. M. Caroff, R. C. Maury, J. Leterrier, J. Joron, et al., "Trace Element Behavior in the Alkali Basalt–Comenditic Trachyte Series from Mururoa Atoll, French Polynesia," Lithos **30**, 1–22 (1993).
14. J. D. DePaolo, A. M. Linn, and G. Schubert, "The Continental Crustal Age Distribution: Methods of Determining Mantle Separation Ages from Sm–Nd Isotopic Data and Application to the South-Western United States," Geophys. Res. **90** (B2), 2071–2088 (1991).
15. G. N. Eby, "Monteregian Hills. II. Petrography, Major and Trace Element Geochemistry and Strontium Isotopic Chemistry of the Eastern Intrusions: Mounts Shefford, Brome and Megantic," J. Petrol. **26** (2), 418–448 (1985).
16. G. N. Eby, "The A-type Granitoids: a Review of their Occurrence and Chemical Characteristics and Speculations on their Petrogenesis, Lithos **26** (1–2), 115–134 (1990).
17. *Endogenous Regimes and Magmatic Evolution in the Early Precambrian: Evidence from the Northeastern Baltic Shield*, Ed. by I. D. Batieva and A. N. Vinogradov (Nauka, St. Petersburg, 1991) [in Russian].
18. Zh. A. Fedotov and Yu. V. Amelin, "Post-Svecofennian Dolerite Dikes of the Kola Region: Dual Nature of the Cratonic Magmatism," Vestn. MGTU. Tr. Murm. Gos. Tekhn. Univ. **1** (3), 33–41 (1998).
19. H. Fujimaki and M. Tatsumoto, "Partition Coefficients of Hf, Zr and REE between Phenocrysts and Groundmass," in *Proceedings of the 14th Lunar Planetary Science Conference*, Geophys. Res. **89**, 662–672 (1984).

20. M. S. Ghiorso, M. Hirschmann, and R. O. Sack, "MELTS: Software for Thermodynamic Modeling of Magmatic Systems," EOS **75**, 571–576 (1994).

21. E. Hanski and V. F. Smolkin, "Iron and LREE-enriched Mantle Source for Early Proterozoic Intraplate Magmatism as Exemplified by Pechenga Ferropicrites, Kola Peninsula, Russia," Lithos **34**, 107–125 (1995).

22. K. T. M. Johnson, "Experimental Determination of Partition Coefficients for Rare Earth and High-Field-Strength Elements between Clinopyroxene, Garnet, and Basaltic Melt at High Pressures," Contrib. Mineral. Petrol. **133**, 60–68 (1998).

23. L. N. Kogarko, V. A. Kononova, M. P. Orlova, and A. Wooley, *Alkaline Rocks and Carbonatites of the World: 2. Former USSR* (Chapman, London, 1995).

24. S. G. Krivdik and V. I. Tkachuk, *Petrology of Alkaline Rocks in the Ukrainian Shield* (Naukova dumka, Kiev, 1990) [in Russian].

25. A. A. Kukharenko, A. G. Bulakh, G. A. Il'inskii, et al., "Metallogenic Features of the Alkaline Associations of the Eastern Baltic Shield," in *Tr. Leningr. O-va Ispyt. Prir.* **72** (2), 1971.

26. T. C. Liew and A. W. Hofmann, "Precambrian Crustal Components, Plutonic Associations, Plate Environment of the Hercynian Fold Belt of Central Europe: Indications from a Nd and Sr Study," Contrib. Mineral. Petrol. **98**, 129–138 (1998).

27. W. F. McDonough, S. Sun, A. E. Ringwood, E. Jagoutz, et al., "K, Rb, and Cs in the Earth and Moon and the Evolution of the Earth's Mantle," Geochim. Cosmochim. Acta. **56**, 93–101 (1991).

28. F. P. Mitrofanov, V. I. Pozhilenko, V. F. Smolkin, A. A. Arzamastsev, et al., *Geology of the Kola Peninsula, (Baltic Shield)* (Kol'sk. Nauch. Ts., Apatity, 1995).

29. F. P. Mitrofanov, V. F. Smol'kin, and N. V. Sharov, "Main Features of the Geological Structure of the Northeastern Baltic Shield" in *Kola Superdeep. Scientific Results and Investigation Experience*, Ed. by V. P. Orlov and N. P. Laverov (TEKhNONEFTEGAZ, Moscow, 1998) [in Russian].

30. P. Montero and F. Bea, "Accurate Determination of $^{87}Sr/^{86}Sr$ and $^{143}Nd/^{144}Nd$ Ratios by Inductively Coupled Plasma Mass Spectrometry in Isotope Geoscience: an Alternative to Isotope Dilution Analysis," Anal. Chim. Acta **358**, 227–253 (1998).

31. W. P. Nash and H. R. Crecraft, "Partition Coefficients for Trace Elements in Silicic Magmas," Geochim. Cosmochim. Acta. **49**, 2309–2322 (1985).

32. H. O'Brien, T. Ramo, and S. Gehor, *Carbonatite–Kimberlite–Alkaline Rock Field Trip to Southern and Central Finland* (GSF Publ., Espoo, 2004).

33. A. S. Osokin, *Distribution and Composition of the Apatite–Ti-magnetite–Ilmenite Ores of the Gremyakha–Vyrmes Massif* (Kol'sk Fil. AN SSSR, Apatity, 1987) [in Russian].

34. A. A. Polkanov, N. A. Eliseev, E. N. Eliseev, and G. I. Kavardin, *Gremyakha–Vyrmes Massif at the Kola Peninsula* (Nauka, Moscow, 1967) [in Russian].

35. Yu. D. Pushkarev, *Megacycles and Evolution of the Crust–Mantle System* (Nauka, Leningrad, 1990) [in Russian].

36. M. K. Radchenko and S. A. Rezhenova, "Mineral Evolution in the Early Layered Complex of the Gremyakha–Vyrmes Massif," in *Alkaline Magmatism of the Northeastern Baltic Shield* (Kol'sk. Nauch. Ts. RAN, Apatity, 1990), pp. 56–66 [in Russian].

37. V. M. Savatenkov, R. B. Sulimov, G. N. Goncharov, et al., "Sm–Nd, Rb–Sr and Pb–Pb Isotope Systematics of the Basic–Ultrabasic Rocks in the Gremyakha–Vyrmes Massif: the Role of the Crust–Mantle Interaction in the Magma and Ore Generation," Zap. Vses. Mineral. O-va, No. 5, 15–25 (1998).

38. V. M. Savatenkov, Yu. D. Pushkarev, A. V. Sergeev, and R. B. Sulimov, "Carbonatites as Indicators of New Ore Specialization of the Gremyakha–Vyrmes Massif, Russia," Geol. Rudn. Mestorozhd. **41** (5), 449–454 (1999) [Geol. Ore Dep. **41** (5), 409 (1999)].

39. E. V. Sharkov and V. F. Smolkin, "Palaeoproterozoic Layered Intrusions of the Russian Part of the Fennoscandian Shield: A Review," Trans. Inst. Min. Metall. Sect. B: Appl. Earth Sci. **107**, B23–B38 (1998).

40. V. F. Smol'kin, "Magmatism of the Early Proterozoic (2.5–1.7 Ga) Rift System in the Northwestern Baltic Shield," Petrologiya **5** (4), 394–411 (1997) [Petrology **5** (4), 350 (1997)].

41. V. F. Smol'kin, *Early Precambrian Komatiite and Picrite Magmatism of the Baltic Shield* (Nauka, St. Petersburg, 1992) [in Russian].

42. M. J. Timmerman and J. S. Daly, "Sm–Nd Evidence for Late Archaean Crust Formation in the Lapland–Kola Mobile Belt, Kola Peninsula, Russia and Norway," Precambr. Res. **72**, 97–107 (1995).

43. V. R. Vetrin, O. M. Turkina, and O. Nordgulen, *Surface Analogues of "Grey Gneiss" among the Archaean Rocks in the Kola Superdeep Borehole* (Kola Science Centre RAS, Apatity, 1999).

44. A. N. Vinogradov, I. D. Batieva, I. V. Bel'kov, and G. V. Vinogradova, "Petrochemical Types and Formation Sequence of the Intrusive Series in the Polyformational Gremyakha–Vyrmes Massif, Kola Peninsula," in *Petrology and Metallogeny of the Alkaline, Alkaline–Ultramafic, and Carbonatite Complexes of the Karelian–Kola Region* (Kol'sk. Fil. AN SSSR, Apatity, 1985), pp. 3–12 [in Russian].

45. G. L. Vursii, T. B. Bayanova, and N. V. Levkovich, "Structure and Age of the Gremyakha–Vyrmes Ultrabasic–Basic Pluton," in *Proceedings of the 1st All-Russia Conference on Isotope Geochronology. Isotope Dating of the Geological Processes: New Methods and Results. Moscow, Russia, 2000* (GEOS, Moscow, 2000), pp. 99–100 [in Russian].